Radiative Forcing of a Tropical Direct Circulation by Soil Dust Aerosols

R. L. MILLER AND I. TEGEN

Department of Applied Physics, Columbia University, and
NASA/Goddard Institute for Space Studies, New York, New York

(Manuscript received 18 December 1997, in final form 27 August 1998)

ABSTRACT

The effect of soil dust aerosols upon the tropical climate is estimated by forcing a simple model of a tropical direct circulation. The model consists of a region vertically mixed by deep convection and a nonconvecting region, for which budgets of dry static energy and moisture are constructed. Dynamical effects are included implicitly, by prohibiting horizontal temperature contrasts above the boundary layer.

Dust aerosols absorb sunlight to a greater extent than industrial sulfate and sea-salt aerosols. In a companion study, where the climate response to dust is calculated using an atmospheric general circulation model, the global-average dust radiative forcing is negligible at the top of the dust layer, in comparison to the large reduction of the net flux at the surface. Thus, dust aerosols redistribute radiative heating from the surface into the dust layer, unlike industrial sulfates and sea salt, which through reflection reduce the total radiative energy gained by the column.

The simple model is perturbed by a reduction in the net radiative flux at the surface. Forcing at the top of the dust layer is idealized to be zero. Cooling occurs at the surface of the nonconvecting region, but surface temperature within the convecting region is only slightly perturbed. It is shown that the disproportionately small response within the convecting region is a consequence of the trivial radiative forcing at the top of the dust layer, and the occurrence of deep convection, which prevents the surface temperature from changing without a corresponding change of the emitting temperature in the upper troposphere.

Additional experiments, where the absorptivity of the dust particles is varied, indicate that the anomalous surface temperature is most sensitive to the radiative forcing at the top of the dust layer. The reduction of the surface net radiation is less important per se but introduces an asymmetry in the response between the convecting and nonconvecting regions through the radiative forcing within the dust layer, which is the difference between the forcing at the surface and the layer top. This heating can offset radiative cooling above the boundary layer, reducing the strength of the circulation that links the nonconvecting and convecting regions. The weakened circulation requires cooling of the nonconvecting region relative to the convecting region in order to maintain the export of energy from the latter to the former.

It is suggested that the ''semi-indirect'' effect of aerosols, wherein cloud cover is changed in response to aerosol heating, is sensitive to the vertical extent and magnitude of the aerosol forcing.

The experiments suggest that dust optical properties (to which the top of the atmosphere forcing is sensitive) should be allowed to vary with the mineral composition of the source region in a computation of the climate response. More extensive measurements of the dust optical properties, along with the vertical distribution of the dust layer, are needed to reduce the uncertainty of the climate response to dust aerosols.

1. Introduction

Radiative forcing by anthropogenic aerosols exceeds the forcing by anthropogenic CO_2 in certain regions and may obscure the climate ''fingerprint'' attributed to the latter (Mitchell et al. 1995). Industrial sulfate aerosols have received much attention, but soil dust, being more abundant, has a greater radiative effect in certain regions (Li et al. 1996) and a comparable effect globally (Sokolik and Toon 1996; Tegen et al. 1997). Soil dust aerosols are created by the wind erosion of dry soil. While dust concentrations are largest near desert and semiarid regions, the smallest particles, which have the largest cross-sectional area per unit mass and thus the largest radiative effect, remain suspended in the atmosphere for a week or more (Tegen and Fung 1994) and can be swept thousands of kilometers downwind from the source region. Dust from the Sahara and Sahel regularly crosses the Atlantic, as revealed by direct measurement at Barbados (e.g., Prospero and Nees 1986) and satellite images (e.g., Husar et al. 1997; Moulin et al. 1997; Herman et al. 1997). During the Northern Hemisphere (NH) summer, a dust aerosol plume extends from the Caribbean, across the Sahara and Arabian deserts, to the Chinese loess deposits and the Pacific coast of Asia

Corresponding author address: R. L. Miller, Department of Applied Physics, Armstrong 550, Columbia University, New York, NY 10027.
E-mail: rlm15@columbia.edu

(e.g., Tegen and Fung 1994). Roughly half of the atmospheric dust is estimated to be the result of human activities such as agriculture, overgrazing, and deforestation (Tegen and Fung 1995), so the anthropogenic component of dust radiative forcing is potentially large (Tegen et al. 1996).

Soil dust aerosols absorb solar radiation to a greater extent than industrial sulfates (Lacis and Mishchenko 1995; Tegen and Lacis 1996). While reduction of the net surface flux by sulfates occurs through reflection of sunlight and is accompanied by a decrease in the net flux entering the atmospheric column, reduction of the surface flux by soil dust occurs to a greater extent through the absorption of sunlight within the dust layer, leaving the column radiation gain relatively unchanged.

To calculate the effect of radiative forcing by soil dust aerosols upon climate, Miller and Tegen (1998) compared two atmospheric general circulation model (AGCM) simulations, one of which included soil dust. The mean seasonal distribution of atmospheric dust was prescribed, based upon estimates derived from an offline chemical tracer model coupled to a specified surface distribution of soil particle sizes (Tegen and Fung 1994, 1995). In response to radiative forcing by dust aerosols, AGCM surface air temperatures typically decrease on the order of 1 K beneath the dust layer, as well as certain regions outside of the dust cloud. However, cooling does not occur everywhere beneath the region of large aerosol concentration. Surface air temperatures are nearly unchanged within regions of frequent deep convection, such as the Arabian Sea during NH summer, even though the surface net radiation in this region is reduced by as much as 60 W m^{-2}.

This lack of response resembles behavior described by Cess et al. (1985), who forced a single-column radiative-convective model and an AGCM with radiative forcing corresponding to absorbing aerosols associated with a ''nuclear winter'' scenario. For moderate aerosol concentrations, the absence of surface cooling is attributed to the small perturbation to the net radiative gain at the top of the atmosphere (TOA), which is a stronger constraint than the large reduction in the net surface flux. This interpretation is based upon a single-column model or else on hemispheric-scale averages in the AGCM, and several questions arise when applying it to the regional-scale variations in surface temperature found by Miller and Tegen (1998) for the Arabian Sea and its surroundings. For example, it is not immediately apparent why the radiative gain at TOA has exclusive control of temperature at the surface, since the dynamical export of energy to adjacent regions may be altered by the dust radiative heating; indeed, we show that this heating reduces the strength of the circulation linking a convecting region and its surroundings. It also remains to be explained why surface cooling occurs in regions surrounding the Arabian Sea, where the TOA forcing is comparable and the surface forcing is smaller. A related question is why dust aerosols are able to cool the surface of the Arabian Sea during NH winter, despite smaller forcing in this season.

In this study, we consider the effect of radiative forcing by soil dust aerosols upon a simple model of a tropical direct circulation, in order to understand why the surface response of the AGCM is not more uniform beneath the aerosol layer and is typically smallest within the convecting region. By ''Tropics,'' we refer to the region between roughly 30°S and 30°N—essentially the domain of the Hadley circulation—and thus include the subtropics in addition to the deep Tropics. The interaction of dust radiative heating with a tropical circulation is of interest because much of the observed dust originates in the vicinity of subtropical deserts so that atmospheric dust concentrations are especially high at low latitudes (e.g., Tegen and Fung 1994). The simple model is a useful complement to the AGCM calculation of Miller and Tegen (1998), because it removes the competing sources of variability that are present in the AGCM, allowing the mechanism by which dust perturbs the climate to be identified. This in turn allows us to suggest aspects of the AGCM response that are robust and would be expected to appear in calculations with other climate models. In addition, we will use the simple model to estimate the climate sensitivity to certain aspects of the dust forcing that are poorly constrained by measurements, such as the optical properties of dust particles and the vertical extent of the dust cloud, through experiments that be would prohibitively expensive with the full AGCM.

In section 2, we describe our model of a tropical direct circulation, along with the unperturbed climate prior to the imposition of dust radiative forcing. The model consists of budgets of dry static energy and moisture, with the effects of dynamics treated implicitly. The model was originally developed to study the interaction between subtropical low clouds and the Hadley–Walker circulation (Miller 1997) and is based upon the simple thermodynamic models of Sarachik (1978), Betts and Ridgway (1989), and Pierrehumbert (1995). The model divides the Tropics into a region well mixed by deep convection and a descending region where convection is absent. By prescribing the dust radiative forcing in each region, we can examine whether each atmospheric column adjusts in isolation from its neighbors, and whether the circulation linking adjacent regions leads to an asymmetry in the response.

In section 3, we consider the mechanism by which the atmosphere responds to dust radiative forcing and balances the competing effects of a large reduction in the surface net radiative flux with a comparatively small TOA perturbation. While the TOA forcing is revealed to be a strong constraint upon the response within the convecting region, a result consistent with Cess et al. (1985), the response within the nonconvecting region depends upon the perturbation by dust radiative heating to the circulation linking the two regions. A reduction in circulation leads to greater cooling in the noncon-

vecting region, as occurs in the AGCM experiments of Miller and Tegen (1998). We also consider how the substantially reduced surface radiative flux is compensated in the surface energy balance without large cooling of the air at this level, and to what extent the climate response depends upon the presence of an ocean or continental surface as a lower boundary.

In section 4, we consider the sensitivity of the model response to changes in the dust radiative properties along with the height of the aerosol layer, aspects of the forcing that are uncertain due to limited measurements. In the final section, we present our conclusions and identify observations that are needed to reduce the uncertainty in the climate response to dust aerosol forcing.

2. Model description

The simple model of a tropical direct circulation, developed by Miller (1997) to study the interaction of the Hadley–Walker circulation with subtropical marine stratus cloud cover, is based upon the tropical models of Sarachik (1978), Betts and Ridgway (1989), and Pierrehumbert (1995), which consist of area-averaged thermodynamic budgets, along with implicit dynamical constraints, as described below. [A similar approach is used in the steady-state hurricane model of Emanuel (1986).] As described in detail in Miller (1997), budgets are constructed of dry static energy $s = C_pT + gz$, specific humidity q, and liquid water l. The budget equations are given in the appendix. Here we describe the model in general terms, while noting changes made for the purposes of this study.

The model is intended to represent the Hadley–Walker circulation and divides the Tropics into a region vertically mixed by deep convection and a nonconvecting region characterized by descent. The two regions are linked by a circulation that exits the convecting region at the tropopause and subsides within the nonconvecting region in order to balance radiative cooling [Eq. (A6)]. For simplicity, the rate of descent is assumed to be constant between the tropopause and the lifting condensation level, below which air returns to the convecting branch. Within the convecting region, ascent and the release of latent heat occur in isolated updrafts, which are meant to represent convective cloud clusters (Houze and Betts 1981). Between the updrafts, radiative cooling is again balanced by subsidence [Eq. (A5)]. The circulation is illustrated in Fig. 1.

The division of the convecting region into updrafts embedded in subsiding air is motivated by observations (e.g., Riehl and Malkus 1958) that show that deep convective cloud cover and ascent occur within only a small fraction of the Tropics at any one time—roughly 5% according to International Satellite Cloud Climatology Project (ISCCP) estimates (e.g., Miller 1997). However, the location of these updrafts varies, so that on a longer timescale of a few weeks or more, a much larger fraction of the Tropics—roughly 40%—is vertically mixed by

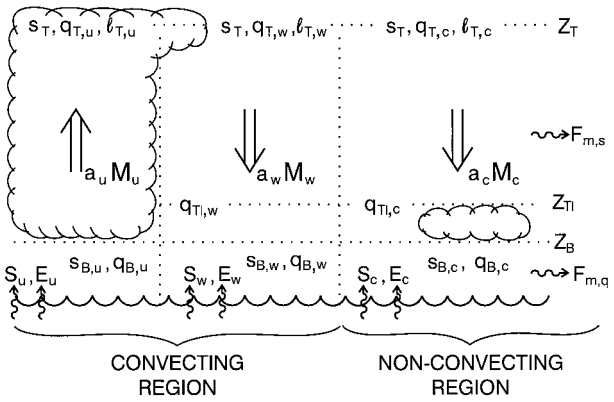

FIG. 1. A schematic of a simple model of the Tropics. Air detrains from the convective updraft at the tropopause z_T, descends through the trade inversion at z_{TI}, and returns to the updraft within the mixed layer of thickness z_B corresponding to the lifting condensation level. At the tropopause, there is a mass flux a_uM_u from the updraft to the convecting region, and a flux a_cM_c from the convecting region to the nonconvecting region, with equal and opposite flow below within the mixed layer.

deep convection. As a consequence of the isolated updrafts, subsidence occurs in the model not only within the nonconvecting region, but also within a large fraction of the convecting branch.

The small areal extent of observed updrafts allows the model equations to be simplified by approximating the updraft area as zero, as described in Miller (1997). (The total flux of mass within the updraft, equal to the product of the updraft area and the rate of ascent, remains nonzero in this limit.) Then, the moist static energy of air at the surface of the convecting region and the tropopause are necessarily equal [Eq. (A1)]. This idealization of vanishing updraft area is implicit in the models of Sarachik (1978) and Betts and Ridgway (1989).

Dynamical effects are introduced into the model by assuming that above the boundary layer (defined below), horizontal contrasts of temperature are eliminated by the large-scale circulation. For a symmetric circulation, this constraint can be derived by assuming that air detraining from the convective towers conserves angular momentum as it travels poleward (Schneider 1977; Held and Hou 1980). This determines the zonal wind, which together with the thermal wind equation implies the absence of horizontal temperature contrasts above the boundary layer (Fang and Tung 1996). Note that this vanishing gradient is independent of the radiative forcing, so long as the poleward circulation conserves angular momentum and is in thermal wind balance. The effect of the radiative forcing manifests itself upon the strength of the mean meridional circulation needed to maintain the temperature gradient required by these two constraints (Held and Hou 1980). While this argument strictly holds only for a zonally symmetric circulation, the Rossby radius of deformation, over which a direct circulation smoothes out temperature gradients, is larg-

est at the equator, so that the assumption of horizontally uniform temperature is expected to apply to the Walker circulation as well.

While the temperatures of the convecting and nonconvecting regions are taken to be identical above the boundary layer, there are differences in the assumed moisture content between the two regions. Moisture enters the model's hydrologic cycle by evaporating at the surface and traveling toward the convective clusters within the lower branch of the direct circulation, which represents the trade winds [Eqs. (A7), (A8)]. Within the updraft, a large fraction of the moisture condenses and falls to the surface as precipitation [Eq. (A15)]. The remainder detrains as hydrometeors at the tropopause (mostly ice crystals) and reevaporates while subsiding back toward the surface air [Eqs. (A9)–(A14)]. Analyses of radiosonde humidity by Sun and Oort (1995) demonstrate that upper-tropospheric specific humidity increases with surface air temperature within regions of frequent deep convection but is relatively unchanged where convection is absent. Based upon this analysis, we relate upper-tropospheric moisture within the convecting branch to the surface relative humidity as in Manabe and Weatherald (1967). In contrast, moisture within the nonconvecting branch is fixed at some prescribed value. In reality, subtropical moisture depends upon reevaporation of hydrometeors along with lateral advection by both the symmetric and asymmetric components of the tropical circulation (Sun and Lindzen 1993; Salathe and Hartmann 1997; Yang and Pierrehumbert 1994; Pierrehumbert 1998). This lateral transport is quite sensitive to the vertical dependence of the mass flux and upwind moisture (Larson et al. 1999). The main obstacle to computing subtropical upper-tropospheric moisture in the current study is the need to know how the mass flux and moisture are perturbed by the dust radiative heating. This requires, at minimum, a precise estimate of the vertical distribution of this heating, which, as noted in later sections, is poorly constrained by observations. We will discuss the effect of assuming fixed moisture within the nonconvecting branch in greater detail in the next section.

Figure 1 summarizes the division of the Tropics into a nonconvecting region and a convecting region with embedded updrafts. Subsidence occurs within the nonconvecting region, along with virtually all of the convecting region. However, subsiding air within the convecting region is distinguished by its high moisture content, a result of its proximity to the updrafts.

In Miller (1997), the direct circulation was assumed to lie above an ocean surface. Consequently, variables corresponding to the convecting region were denoted by the subscript *w* for ''warm pool,'' while variables in the nonconvecting region were denoted by *c* for ''cold pool.'' For the sake of consistency, this subscript notation will be used in the present study. However, because we will extend this model to direct circulations over land, we will generally use the term ''convecting region'' for warm pool, along with ''nonconvecting region'' for cold pool.

a. Vertical structure

We divide each region into two layers—a boundary layer and the overlying free troposphere—and construct budgets of dry static energy and moisture integrated over the depth of each layer. These budgets yield surface and tropopause values of these variables, which are depicted in Fig. 1. We then interpolate these variables throughout the remainder of the column, based upon the observed vertical structure of the tropical atmosphere, as described below. While climate feedbacks involving subtle changes in the vertical structure elude our model, such an approach yields a realistic tropical climate (e.g., Sarachik 1978; Betts and Ridgway 1989; Pierrehumbert 1995; Miller 1997), and its simplicity facilitates the physical interpretation of our solutions.

Within the free troposphere, temperature is given by the moist adiabat that originates at the surface of the convecting region. Betts (1982) and Xu and Emanuel (1989) show that this is a good approximation for regions of frequent deep convection. For extreme concentrations of absorbing aerosols, characteristic of nuclear winter scenarios, the temperature of surface parcels can be reduced to the point that they are no longer upwardly buoyant and effective at maintaining a convectively neutral profile (Cess et al. 1985). For example, the West African monsoon circulation collapses in the nuclear winter AGCM experiments of Ghan et al. (1988). In this case, a direct circulation is reestablished higher in the atmosphere, originating at a level where the dust radiative heating is largest. However, for the observed concentration of soil dust aerosols, convection persists in the AGCM experiments of Miller and Tegen (1998), and the tropical lapse rate is nearly unchanged. As noted above, the absence of horizontal temperature contrasts above the boundary layer means that the same adiabat is used to prescribe upper-tropospheric temperature within the nonconvecting region.

Within the boundary layer, air between the surface and lifting condensation level (denoted by z_B in Fig. 1) is assumed to be well mixed by dry convection, resulting in uniform values of potential temperature and moisture. Between the lifting condensation level and the trade inversion (z_{TI} in Fig. 1), thermodynamic variables are assumed to represent a mixture of air from below with air subsiding through the trade inversion, as in Betts and Ridgway (1989). The trade inversion height is specified, as in Miller (1997). Within the convecting region, z_{TI} is set at 2 km, while within the nonconvecting region, the inversion is set at 1.5 km for the oceanic case. For the continental case, the top of the boundary layer within the nonconvecting region is calculated as described below.

In contrast to Miller (1997), where the surface fluxes of latent and sensible heat were calculated in order to

maintain a prescribed surface relative humidity and air–sea temperature difference, surface fluxes in this study will be prescribed using bulk formulas:

$$LE = \beta L\omega_0[q^*(\mathrm{SST}) - q_B]$$
$$S = C_P\omega_0(\mathrm{SST} - T_s), \quad (1)$$

where L is the latent heat of vaporization for water, E is the evaporation rate, and S is the surface sensible heat flux. In addition, C_P is the specific heat of air at constant pressure; β is the evaporation efficiency (equal to the actual evaporation rate divided by the evaporation rate were the moisture supply of the ground unlimited); and ω_0 is a bulk coefficient, equal to the product of the air density ρ, a drag coefficient C_D, and a typical surface wind speed. The quantity q^*(SST) is the saturation specific humidity evaluated at the sea surface temperature (SST), or else the ground temperature, while T_s and q_B, respectively, are the temperature and specific humidity of the surface air.

We will use both a land surface and ocean as a lower boundary for the model. Over land, evaporation is limited by the available soil moisture. One simple way of parameterizing this effect is by means of a ''bucket'' model, a common land surface parameterization in early AGCMs (e.g., Hansen et al. 1983). In this type of parameterization, the evaporation efficiency β in (1) is set equal to the ratio of the soil moisture to the moisture capacity of the soil, and is thus at most unity, when the soil is completely saturated. It is beyond the intent of this model to compute the soil moisture. Instead, we will prescribe values of the evaporation efficiency appropriate to various land surface types, derived from the AGCM experiments of Miller and Tegen (1998). Over the ocean, β is set equal to unity. For the continental case, β is set equal to 0.5 beneath the convecting region, a value characteristic of the verdant Guinea coast of West Africa, whereas in the nonconvecting region, β is given smaller values between 0.15 and 0.01 that are more typical of the deserts to the north.

As β is reduced within the nonconvecting region to values characteristic of semiarid and desert regions, the surface relative humidity decreases and the lifting condensation level rises. For these extreme cases, the assumption of a cloudy layer consisting of a mixture of surface and desert air is inappropriate. For example, Carlson and Prospero (1972) show a midday summertime radiosonde profile for Tamanrasset on the western fringe of the Sahara, which demonstrates that the dry convective surface layer extends as high as 500 mb, with no cloudy air above. For the continental case, we assume a different boundary layer structure in the nonconvecting region, whereby the region between the surface and the free troposphere consists of a single layer well mixed by dry convection. The height of this layer is computed by requiring that the temperature be continuous with the free-tropospheric value above. While the large-scale circulation will attempt to eliminate horizontal temperature contrasts resulting from the contrasting boundary layer depths in convecting and nonconvecting regions (Schubert et al. 1995), we neglect this effect, assuming that the timescale for boundary layer mixing is sufficiently rapid.

b. Unperturbed solution

For the case of a direct circulation overlying an ocean surface, the model is nearly identical to that of Miller (1997), with the only difference in the current study being the use of bulk parameterizations for the surface fluxes through (1). Because the solutions of the two models are nearly identical, we show only the surface air temperature (hereafter abbreviated as ''surface temperature'') and specific humidity in Fig. 2, referring the reader to Fig. 6 in Miller (1997) for other aspects of the solution.

Model solutions are given as a function of the specific humidity in the upper troposphere of the nonconvecting region, q_c at 5 km to be precise. As noted above, observations suggest that moisture above the trade inversion of the nonconvecting region is not well correlated with changes in the convecting region, and we will hold q_c at 5 km fixed when computing the solution, treating it as an external variable of our model as in Miller (1997). In the latter study, specific humidity was specified at the trade inversion at 1.5 km. However, for continental solutions, the boundary layer can extend almost to 5 km for our chosen range of β_c, necessitating the use of a higher reference level. The National Centers for Environmental Prediction reanalyses (Kalnay et al. 1996) suggest that a typical value of specific humidity at 5 km is between 1 and 2 g kg^{-1}.

For a continental direct circulation, surface temperatures in the absence of dust radiative forcing are shown in Fig. 3a, given various choices of β_c, the evaporation efficiency within the nonconvecting region. AGCM estimates of β, computed using the land surface parameterization of Rosenzweig and Abramopoulos (1997), give values typically less than 0.15 for most of Africa north of the Sahel, along with the Middle East, and the southern latitudes of Central Asia. In the driest parts of the Sahara and Arabian deserts, β_c is less than 0.05.

According to Fig. 3a, our model yields solutions with warmer air temperatures within the nonconvecting region. That is, the direct circulation is importing energy *into* the relatively warm nonconvecting region from the cooler convecting region. This behavior may seem surprising at first, and it is worth consideration because it reveals the physics underlying the model, which will prove helpful when interpreting the effect of dust radiative forcing. As noted by Neelin and Held (1987), a direct circulation exports total energy, including the latent component, rather than merely sensible heat and potential energy. Consider the column-integrated budget of total energy for the nonconvecting region, which can be written in terms of the moist static energy:

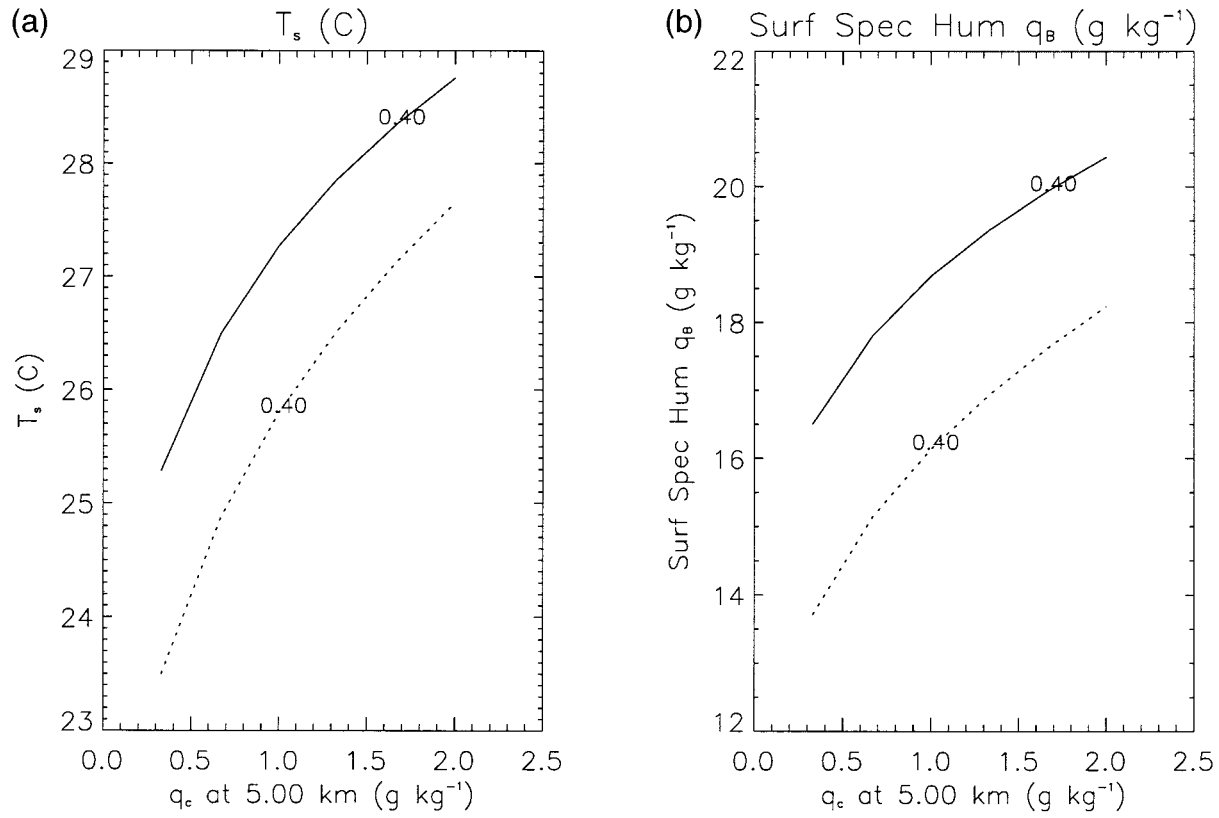

FIG. 2. Equilibrium solution for the convecting region (solid) and nonconvecting region (dashed) of an oceanic direct circulation in the absence of dust radiative heating; (a) surface temperature (°C) and (b) surface specific humidity (g kg^{-1}).

$$h = C_P T + gz + Lq. \quad (2)$$

As described in the appendix, this budget is

$$a_c R_c(z_T) + a_c F_{o,c} + a_c F_{m,h} + a_c M_c(h_T - h_{B,c}) = 0. \quad (3)$$

The first three terms of (3) represent the total loss of energy by the nonconvecting region, consisting of the net radiative loss $a_c R_c(z_T)$ at the tropopause z_T, along with the export of energy by ocean and atmospheric eddy transports, denoted by $a_c F_{o,c}$ and $a_c F_{m,h}$, respectively (a_c represents the fractional area of the nonconvecting region). Balancing this loss is the import of heat from the convecting region by the large-scale circulation. This energy import depends upon the mass flux linking the two regions, proportional to $a_c M_c$ (positive downward), and the difference in moist static energy between air entering the nonconvecting region at the tropopause of the convecting region (characterized by moist static energy h_T) and air leaving the nonconvecting region at the surface (characterized by moist static energy $h_{B,c}$). The quantity $h_T - h_{B,c}$ is identical to the ''gross moist stability'' derived by Neelin and Held (1987), who noted that in order for the direct circulation assumed by our model to export energy gained by the convecting region, the moist static energy must be larger in the outflow branch of the circulation.

The direct circulation can import energy into the warmer region because of the component of latent energy Lq that is advected by the circulation. This is not obvious from (2) and (3), which shows that the net flux of latent energy is actually into the convecting branch, due to the higher humidity at the surface in comparison to the tropopause. However, we can rewrite (3) using the fact that the moist static energy at the tropopause and surface of the convecting region are identical (as a result of the vanishing extent of the updrafts). Then

$$\begin{aligned} &a_c R_c(z_T) + a_c F_{o,c} + a_c F_{m,h} \\ &\quad = -a_c M_c(h_{B,w} - h_{B,c}) \\ &\quad = -a_c M_c[C_P(T_{s,w} - T_{s,c}) + L(q_{B,w} - q_{B,c})], \end{aligned} \quad (4)$$

where T_s and q_B, respectively, are the surface temperature and specific humidity. Ignoring the ocean and atmospheric eddy transports for simplicity, a direct circulation can balance the radiative loss by the nonconvecting region through import of moist static energy, requiring only that the moist static energy at the surface of the convecting region, $h_{B,w}$, be larger than the corresponding value at the surface of the nonconvecting region, $h_{B,c}$. According to (2), the nonconvecting branch of the circulation can be warmer so long as it is sufficiently dry. In terms of (3), the net latent heat flux, albeit toward the convecting region, augments the po-

tential energy at the tropopause and allows the export of total energy into the warmer nonconvecting region. This point was illustrated by Charney (1975), who showed that the Sahara during NH summer *loses* energy to space, and therefore must import it from surrounding regions, even though the desert is relatively warm. Figures 3f and 3h show that the surface moist static energy of the convecting region exceeds that of the nonconvecting region, despite the greater surface temperature of the latter, and that the export of moist static energy out of the convecting region is positive. (The greater moist static energy at the surface of the convecting region—indicating greater column instability—also explains why deep convection persists in this region, despite warmer surface temperatures elsewhere.)

As the soil moisture of the nonconvecting region (related to the evaporation efficiency β_c) is reduced, the local surface temperature warms (Fig. 3a). This feedback has been noted by Walker and Rowntree (1977), with regard to the West African climate. They observe that, as soil moisture decreases, net radiation at the surface is increasingly balanced by the sensible heat flux, rather than through evaporation and loss of latent energy.

While it might be argued that the increased flux of sensible heat warms the air, sensible heating and surface temperature have different (and occasionally opposite) dependencies upon soil moisture, as noted below. Instead, we propose that the rise of surface temperature follows from the near independence of surface moist static energy with respect to soil moisture. Figure 3c shows that the radiation gain at the tropopause of both regions is relatively independent of β_c for all but the smallest values of this parameter. According to (4), the export of moist static energy out of the convecting region must remain the same as β_c changes, as depicted in Fig. 3h. This export is proportional to the mass flux between the two regions, along with the difference in surface moist static energy. The mass flux is given approximately by the radiative cooling between the tropopause and top of the boundary layer, divided by the difference in potential temperature between these two levels [Eq. (A6)]. As long as β_c is not too small, this ratio is nearly constant (Fig. 3g). Thus, the difference in moist static energy between the convecting and nonconvecting regions must stay the same as β_c changes (Fig. 3f). Because the surface of the nonconvecting region dries out as β_c decreases, the surface temperature must rise to maintain the same moist static energy in this region.

Two additional features of the dependence of surface temperature upon soil moisture invite interpretation. First, the surface temperature of the convecting region is nearly independent of soil moisture until β_c passes below 0.05, and then this region actually *cools*, even though air advected from the nonconvecting region is becoming increasingly warm. And second, as β_c decreases below 0.02, the temperature at the surface of the nonconvecting region rises only slightly. (Note also that the rise in surface temperature occurs despite a decrease in the surface sensible heat flux, as shown in Fig. 3i.)

To interpret these features, note that the circulation must emit to space the solar energy that is not transported by atmospheric eddies or ocean currents across its lateral boundaries. Because moisture above the tropical boundary layer is usually large enough to limit direct emission of longwave radiation to space from lower levels, this emission depends mainly upon temperature and moisture in the upper troposphere (e.g., Lindzen et al. 1982; Pierrehumbert 1995). In the convecting region, upper-tropospheric temperature is directly related to the surface value, as a result of deep convection, which maintains a moist-adiabatic lapse rate. Longwave emission in the nonconvecting region is also related to the convecting region surface temperature, as a result of dynamical adjustment, which eliminates horizontal temperature contrasts above the boundary layer. Thus, so long as changes in β_c do not affect the net solar gain at the tropopause, and so long as all longwave emission to space originates above the boundary layer, the surface temperature in the convecting region is necessarily independent of soil moisture in the nonconvecting region.

As the boundary layer warms in response to decreasing soil moisture, we expect that it will increasingly contribute to the outgoing longwave flux at TOA, despite the intervening upper-tropospheric moisture. A signature that this is occurring in the model when β_c becomes as small as 0.02 and 0.01 is that the net radiative loss at the tropopause of the nonconvecting region increases for these values of β_c (Fig. 3c). The net loss at the tropopause is a balance between the net solar flux, longwave emission from the upper troposphere, and emission from lower levels. As the boundary layer of the nonconvecting region warms and dries out, emission from lower levels increases, reducing the upper-tropospheric emission needed to balance the solar flux. However, boundary layer emission only occurs within the nonconvecting region, so that the net radiative gain in the convecting region increases due to the reduced upper-tropospheric emission (Fig. 3c).

This explains why the convecting region cools as β_c becomes as small as 0.02. Reduced upper-tropospheric emission allows upper levels to cool; because the upper-tropospheric emitting temperature is connected by a moist adiabat to the surface value of the convecting region, the surface air cools as well (Fig. 3a). This also explains why the surface temperature of the nonconvecting region increases only marginally as β_c is decreased from 0.02 to 0.01. As the surface of nonconvecting region heats up, it radiates to space much more efficiently. In contrast, at cooler temperatures, energy impinging upon the surface must first be advected to the convecting region and then transported upward before it can escape.

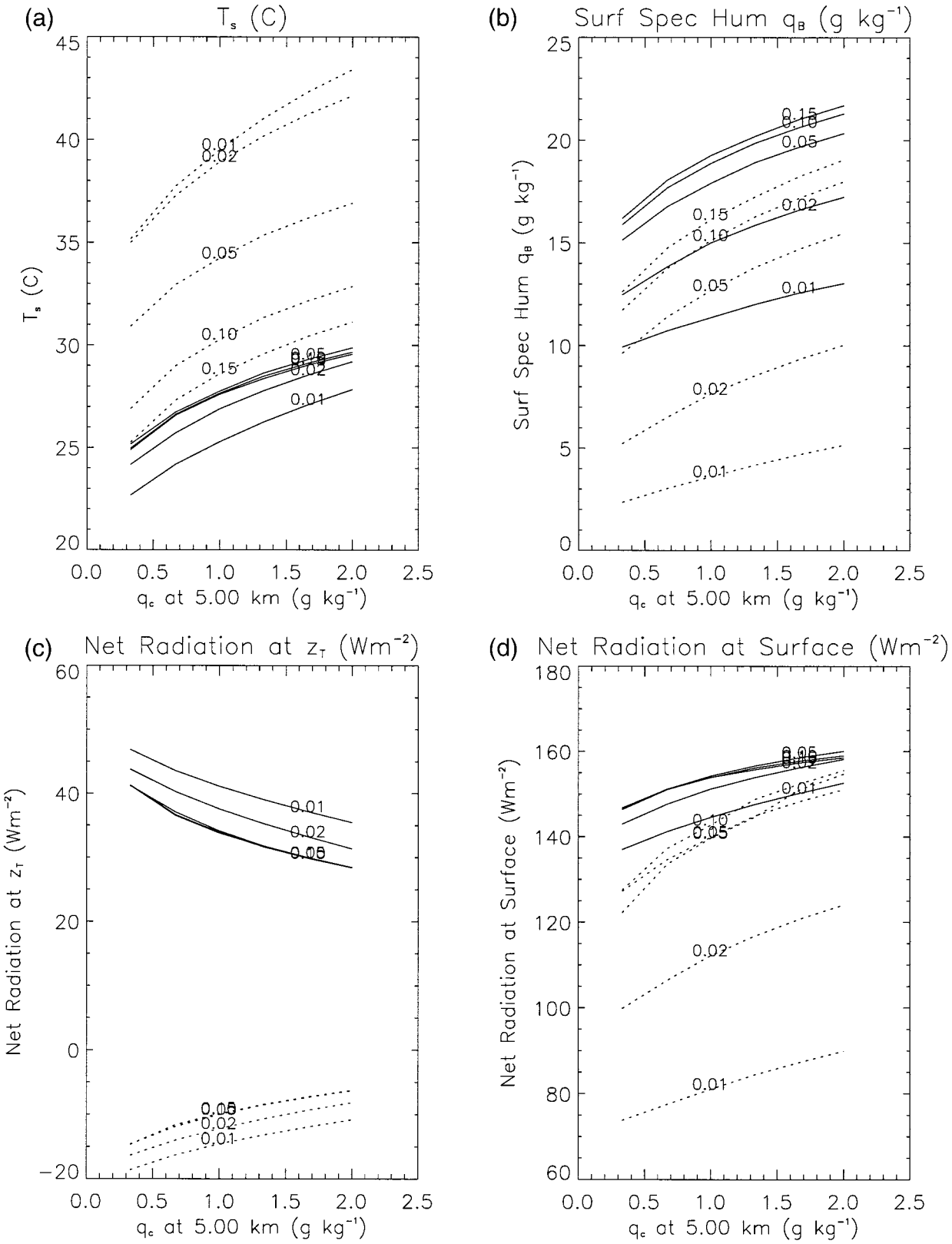

FIG. 3. Equilibrium solution for the convecting region (solid) and nonconvecting region (dashed) of a continental direct circulation in the absence of dust radiative heating, as a function of β_c, the evaporation efficiency at the surface of the nonconvecting region. (a) Surface temperature (°C); (b) surface specific humidity (g kg^{-1}); (c) net radiative gain at the top of the atmosphere (W m^{-2}); (d) net radiative flux at the surface (W m^{-2}); (e) moist static energy scaled by C_P (°C); (f) moist static energy difference between the convecting and

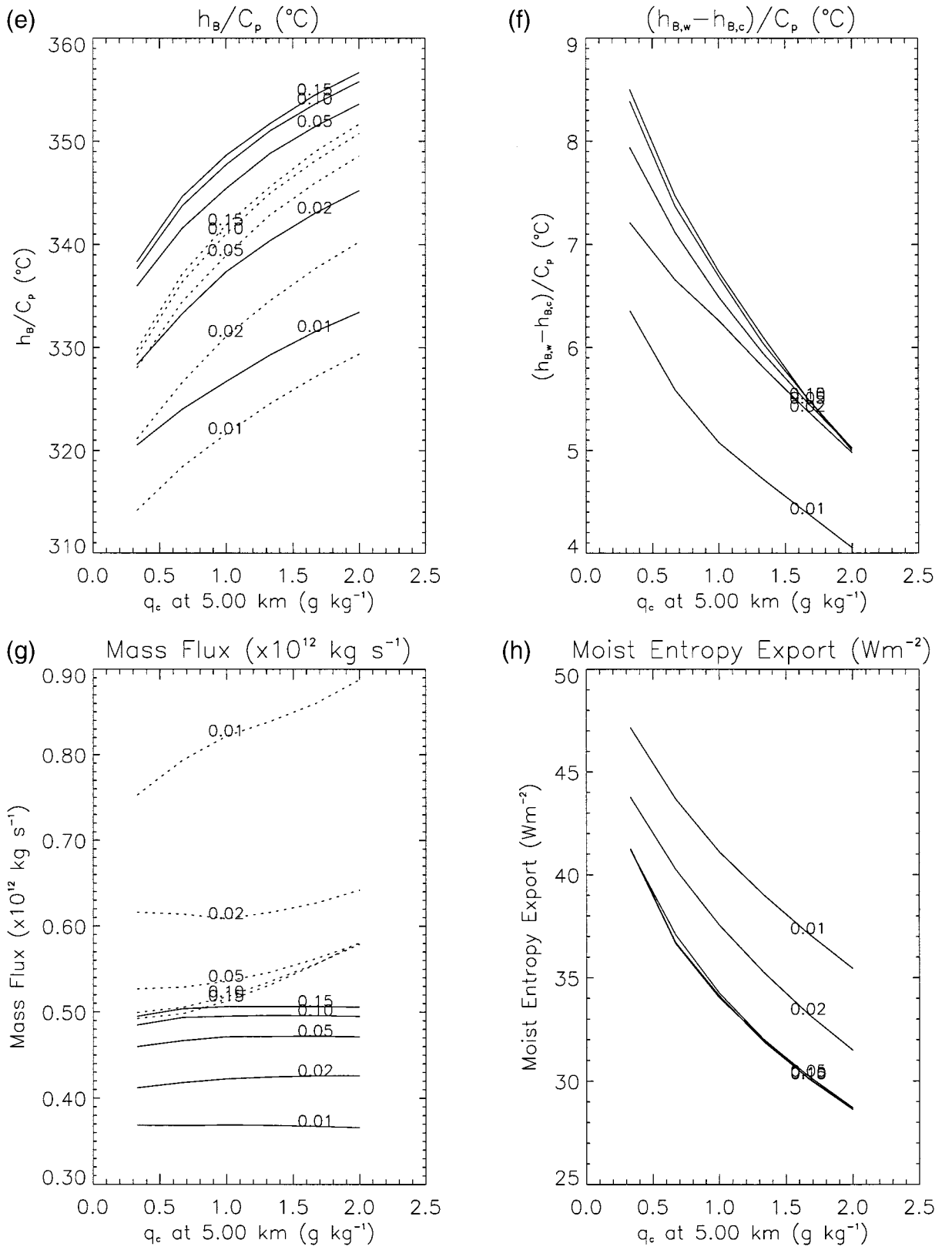

FIG. 3. (*Continued*) nonconvecting regions (°C); (g) area-integrated mass fluxes, i.e., M_w and M_c times the area of the convecting and nonconvecting regions, respectively ($\times 10^{12}$ kg s^{-1}); (h) moist static energy export from convecting region (W m^{-2}); (i) surface sensible heat flux (W m^{-2}); and (j) boundary layer height in the nonconvecting region (m).

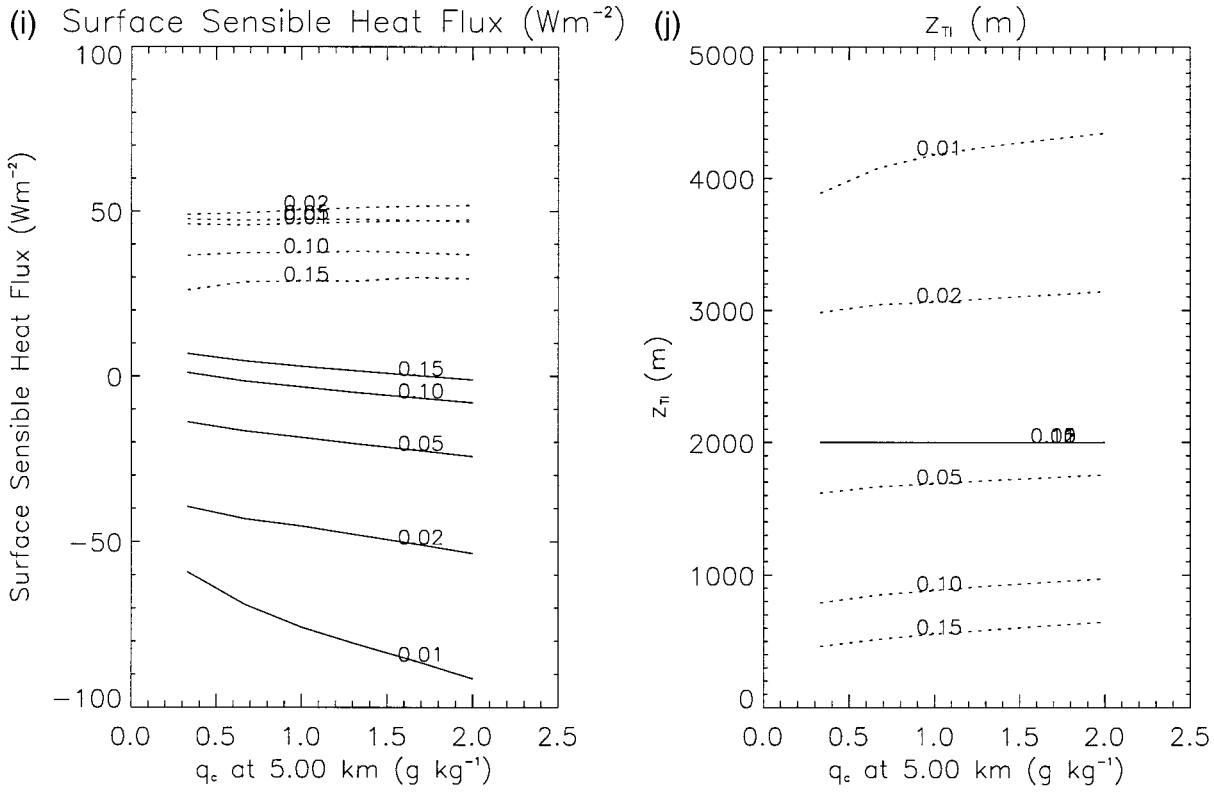

FIG. 3. (*Continued*)

3. Response to dust radiative forcing

In this section, we consider how a tropical direct circulation responds to radiative forcing by soil dust aerosols. Because sunlight is reflected by sulfate aerosols, the reduction of net radiation at the surface is accompanied by a similar decrease in the net flux entering the atmospheric column. In contrast, reduction of surface radiation by dust aerosols occurs to a greater extent through absorption, so that the net radiation entering the column is relatively unchanged. Radiative heating at the surface is displaced into the dust cloud itself.

Increased radiative heating within the atmosphere would by itself drive a direct circulation, causing ascent and precipitation (Eliassen 1951; Schneider 1983). However, the attendant reduction in surface radiation diminishes the surface flux of latent energy (Coakley and Cess 1985), which reduces latent heating within the atmosphere. We consider how the circulation balances these two competing effects. We also consider whether each region adjusts individually to the forcing, or whether the circulation linking adjacent regions is perturbed. We are particularly interested in why the AGCM response to dust radiative heating is disproportionately small in the Arabian Sea during periods of frequent deep convection (Miller and Tegen 1998).

Through its radiative effect, dust perturbs the budget of dry static energy. We include the effect of dust by introducing a radiative anomaly into the model:

$$R_d(p) = R_d(p_{ct}) + \left(\frac{p - p_{ct}}{p_s - p_{ct}}\right)[R_d(p_s) - R_d(p_{ct})], \quad (5)$$

where $R_d(p)$ is the perturbation to the net radiative flux (positive downward) by dust at pressure p; p_{ct} is the pressure at the top of the dust cloud; p_s is the surface pressure; and the radiative perturbation at the surface and cloud-top, $R_d(p_s)$ and $R_d(p_{ct})$, respectively, are to be specified. According to (5), dust radiative heating, proportional to the divergence of the flux, is assumed to be the same at all levels within the dust cloud. Estimated vertical profiles of dust radiative heating (Miller and Tegen 1998; Tegen and Miller 1998) show that this is a reasonable approximation. It is emphasized that we are computing the effect of the climatological distribution of soil dust and not its instantaneous distribution, which can be much more localized with respect to height.

In this section, the dust radiative forcing at the surface $R_d(p_s)$ is set equal to -30 W m^{-2}. This reduction is roughly half the value estimated by Miller and Tegen (1998) for the Arabian Sea during NH summer, and twice the typical value over the entire extent of the summertime dust cloud. At the top of the dust layer,

reflection of sunlight by dust particles is offset by the absorption of upwelling longwave radiation. Consequently, the perturbation by dust to the net radiative flux at this level is small in comparison to the surface reduction, and we idealize the cloud-top value $R_d(p_{ct})$ as zero. Dust particles exhibit a wide range of optical properties (Sokolik and Toon 1996), and in the next section, we consider the sensitivity of the climate response to small changes in the particle properties along with the corresponding TOA forcing.

For the present experiments, the top of the dust cloud is assumed to coincide with the tropopause. During NH summer, frequent deep convection over the Arabian Sea washes out a large fraction of the dust but carries the remainder into the upper troposphere. The vertical distribution is estimated using an offline tracer model as described in Tegen and Fung (1994, 1995), and an improved version of this model predicts a smaller dust concentration at high levels. The vertical extent of dust is also smaller outside of the convecting region. In the next section, we consider the sensitivity of the model response to changes in the height of the dust cloud.

We note that it is the dust radiative forcing that is specified in this model rather than the dust concentration. This distinction is important in principle because the dust radiative forcing can change if the column albedo changes in response to dust, for example, through changes in cloud cover. However, cloud cover is held fixed in this model for the sake of simplicity, so that the distinction is irrelevant here. The fixed radiative anomaly also means that the circulation cannot feed back upon the distribution of dust. Heating of the dust layer by radiative absorption can cause the layer to rise, a process referred to as ''self-lofting'' (Ghan et al. 1988; Browning et al. 1991). However, this effect is relatively small for the heating rates considered here and is neglected.

We first calculate the effect of dust radiative forcing upon a direct circulation overlying an ocean surface, with the goal of understanding the response over the Arabian Sea in the AGCM. Energy transport to midlatitudes by atmospheric eddies and ocean dynamical transports are assumed to remain unperturbed by aerosol forcing. As noted above, the specific humidity in the upper troposphere of the nonconvecting region (q_c at 5 km) is also held fixed, although one could estimate solutions when this parameter is allowed to vary by assuming that the response is nearly linear:

$$\Delta T \approx \left.\frac{\partial T}{\partial R_d}\right|_{q_c} \Delta R_d + \left.\frac{\partial T}{\partial q_c}\right|_{R_d} \Delta q_c. \tag{6}$$

The total change in a quantity, T, in response to dust forcing ΔR_d is equal to the response forced by dust with the upper-tropospheric q_c held constant $\partial T/\partial R_d|_{q_c}\Delta R_d$, plus $\partial T/\partial q_c|_{R_d}\Delta q_c$, the derivative of the unperturbed solution with respect to q_c (estimated from Figs. 2 or 3) times the change in q_c forced by dust.

In the first experiment, the dust layer is assumed to extend across both the convecting and nonconvecting branches of the circulation. The change in surface temperature is shown in Fig. 4a. Cooling at the surface is small in the convecting region, despite the reduction in surface net radiation, but larger within the nonconvecting region.

To understand this response, we first consider why cooling at the surface does not necessarily follow from the large reduction in surface net radiation. Diminished surface radiation is balanced by a reduction in evaporation and the surface latent heat flux and to a lesser extent by a reduced surface sensible heat flux. If we linearize the model's bulk parameterization of evaporation, then

$$LE' = \beta L\omega_0 \left\{ \left[\left.\frac{dq^*}{dT}\right|_{\overline{T}_s} (1 - \overline{r}) + \left.\frac{d^2q^*}{dT^2}\right|_{\overline{T}_s} (\overline{\mathrm{SST}} - \overline{T}_s) \right] T_s' + \left.\frac{dq^*}{dT}\right|_{\overline{T}_s} (\mathrm{SST}' - T_s') - r' q^*(\overline{T}_s) \right\}, \tag{7}$$

where r is the relative humidity of the surface air, an overbar denotes unperturbed quantities, and a prime represents the response to the perturbation. While cooling of the surface air ($T_s' < 0$) can reduce the evaporative flux, this same reduction can be brought about by a decrease in the air–sea temperature difference [$(\mathrm{SST}' - T_s') < 0$] or else an increase in the surface relative humidity ($r' > 0$). To be specific, consider the perturbation to the solution derived with q_c at 5 km set equal to 1.67 g kg^{-1}, where $\overline{\mathrm{SST}}_w$ equals 29.6°C, $\overline{T}_{s,w}$ is 28.4°C, and $\overline{r}_w$ equals 82.4%. Then, for this unperturbed state, which is typical of the Tropics, the relative magnitude of the various feedbacks can be estimated:

$$LE' = 8.7\,\mathrm{W\,m^{-2}\,K^{-1}}\, T_s' + 36.0\,\mathrm{W\,m^{-2}\,K^{-1}}\,(\mathrm{SST}' - T_s') - 6.0\,\mathrm{W\,m^{-2}\,\%^{-1}}\, r'. \tag{8}$$

This shows that a 0.24°C decrease in the air–sea temperature difference or a 0.75% increase in relative humidity is as efficient at reducing the evaporation rate as a 1-K decrease in the surface temperature. In fact (Figs. 4a,c,d), the perturbed values of $T_{s,w}'$, $\mathrm{SST}_w' - T_{s,w}'$, and r_w' are −0.22°C, −0.18°C, and 2.9%, respectively, so that for this case, the reduction in evaporation comes about primarily as a result of the increased relative humidity. We will return to what causes the increased humidity at the surface, despite the reduced evaporation. A reduction in the surface wind speed, a feedback not included in our model, would also act to reduce the evaporation, and we note below that the strength of the circulation is expected to decrease as a result of dust radiative forcing. Thus, the decrease in the evaporative flux, required to compensate the reduction in surface net radiation by dust aerosols, need not lead to cooling at the surface, even though the radiative flux is reduced by as much as 30 W m^{-2} in this case.

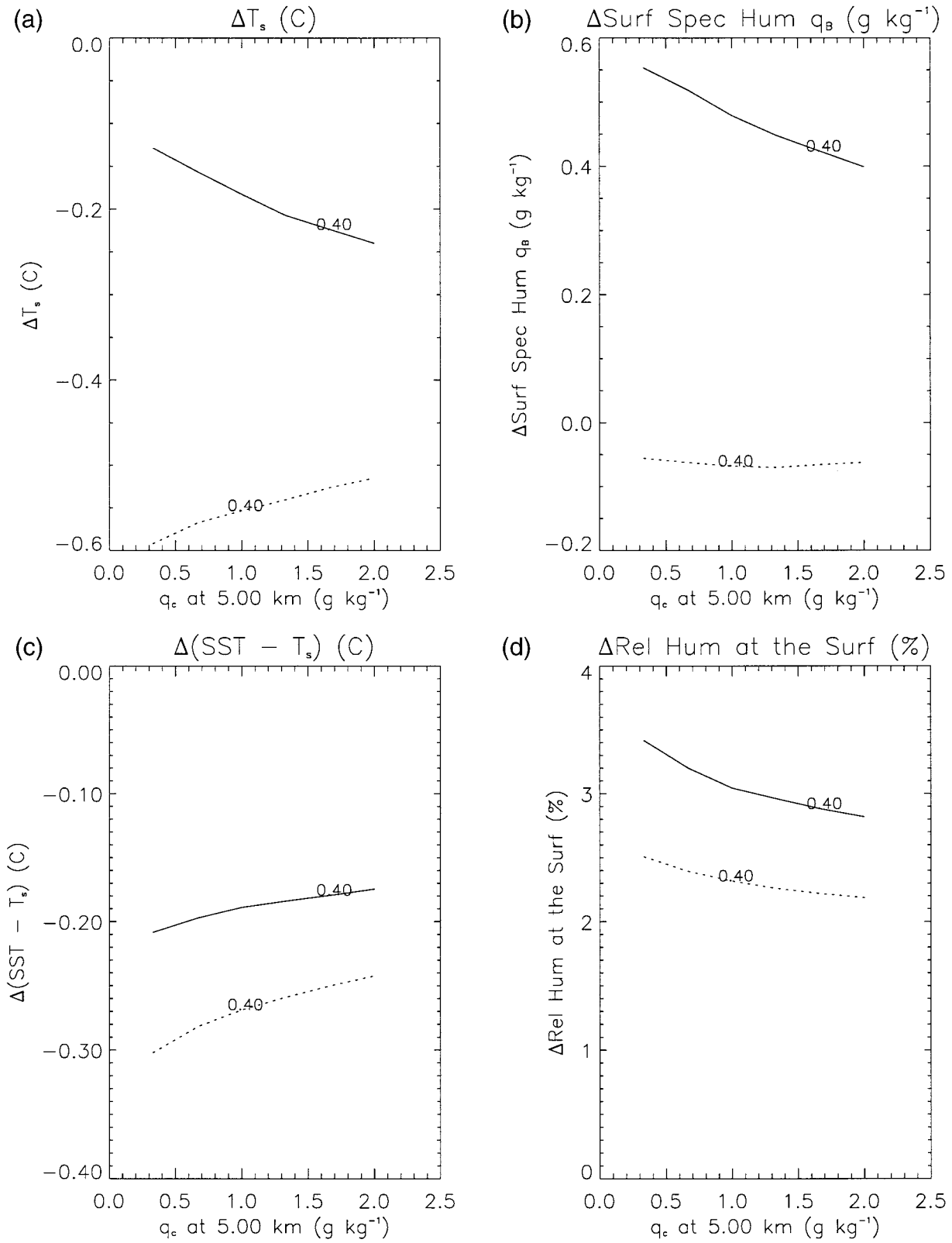

FIG. 4. Perturbation to the solutions for the convecting (solid) and nonconvecting (dashed) regions of an oceanic direct circulation by dust radiative forcing, which is −30 W m^2 at the surface of both regions. (a) Surface temperature (°C); (b) surface specific humidity(g kg^{-1}); (c) sea–air temperature difference (°C); (d) surface relative humidity (%); (e) moist static energy scaled by C_P (°C); (f) area-integrated

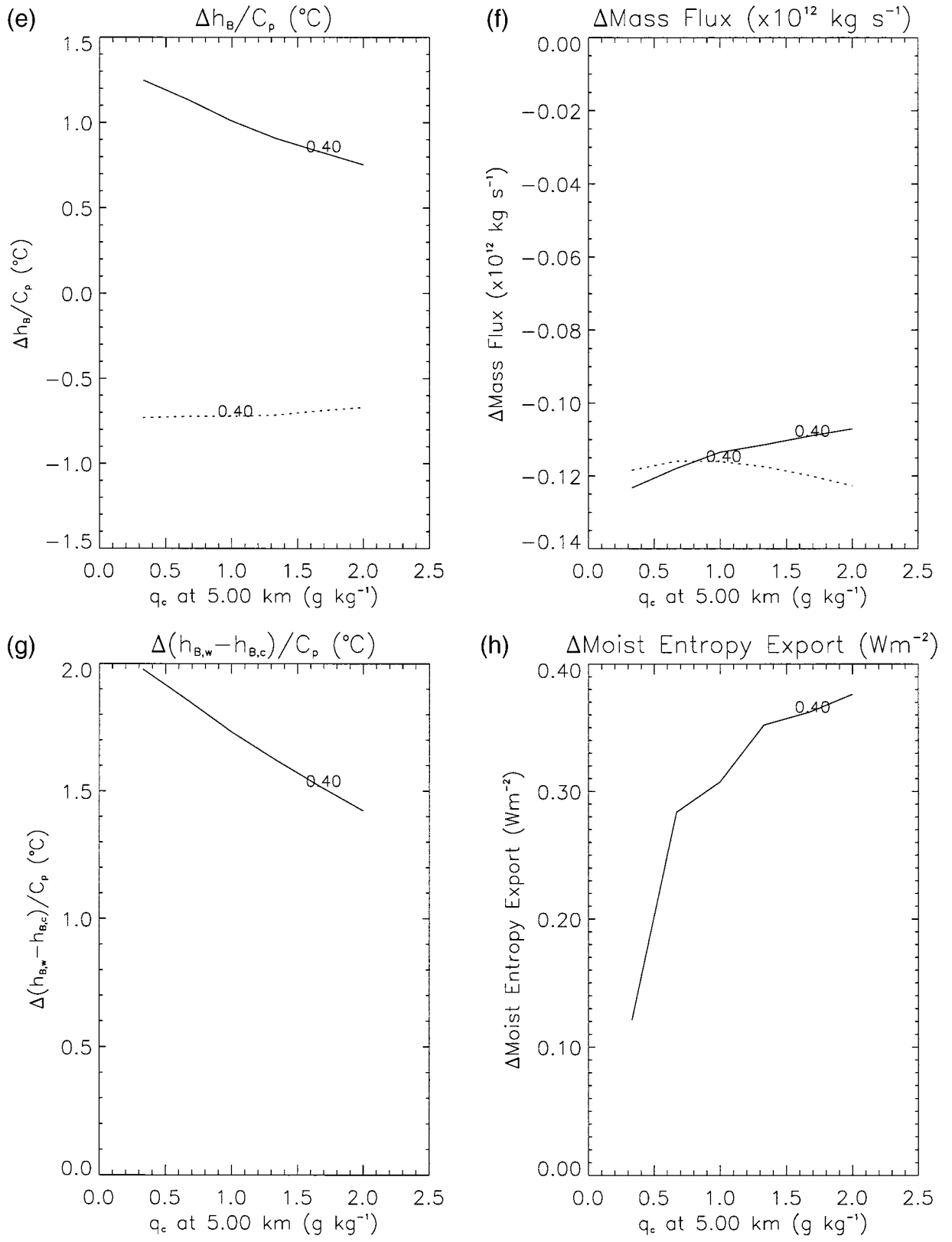

FIG. 4. (*Continued*) mass fluxes, i.e., M_w and M_c times the area of the convecting and nonconvecting regions, respectively ($\times 10^{12}$ kg s^{-1}); (g) moist static energy difference between the convecting + nonconvecting regions (°C); and (h) moist static energy export from convecting region (W m^{-2}).

While cooling at the surface of the convecting region is not required by the large reduction in the surface net radiation, it remains to be seen what prevents this cooling. Cess et al. (1985) observe that for an atmospheric column whose surface temperature is related by deep convective mixing to temperature at other levels, it is the radiative forcing at the top of the atmosphere rather than the surface value that determines the surface temperature anomaly (see also Lindzen et al. 1982). This is because a change in the TOA radiative forcing must be balanced by a change in temperature at the emitting level of the atmospheric column. (A change in the emitter concentration would have the same effect and is considered below.) Because the emitting temperature is related to the surface value by deep convective mixing, the surface temperature is thus constrained by the TOA forcing. This suggests that surface temperature beneath a convecting region, such as the Arabian Sea in the AGCM experiments of Miller and Tegen (1998), is nearly unchanged by dust aerosols because the TOA forcing is nearly zero, and the surface forcing is not strong enough to inhibit convection.

This argument assumes that the column does not adjust to the TOA forcing by exporting energy to adjacent columns through dynamical transports. In principle, the surface of the convecting region could cool, in spite of the trivial dust forcing at TOA, if the corresponding reduction of outgoing longwave radiation (OLR) was balanced by an export of energy to the nonconvecting region and increased longwave emission in the latter. Because of the large-scale circulation, temperature at upper levels of the nonconvecting region is identical to the value within the convecting region. Thus, increased emission of longwave radiation within the nonconvecting region requires warming at upper levels of both regions, which is not possible, given the assumed cooling at the surface of the convecting region. This means that the argument of Cess et al. (1985), based upon a single-column model, can be extended to the convecting region of a tropical circulation, because a change in surface temperature inconsistent with the TOA radiative forcing cannot be compensated by anomalous TOA emission within the surrounding nonconvecting regions.

This behavior is illustrated by the direct circulation model, where dust radiative forcing at TOA is prescribed to be zero, and the net radiative flux at this level changes by less than 1 W m^{-2} for all values of q_c at 5 km (not shown). The small resulting change of temperature at upper levels, related to the change in the moist adiabat, is illustrated by the anomaly of moist static energy at the surface of the convecting region, shown in Fig. 4e. The change in the surface moist static energy is small and in fact is increased slightly by the dust radiative forcing. This increase comes about because the upper troposphere of the convecting region is slightly moistened by dust radiative forcing. This moistening, which by itself would cause a reduction of outgoing longwave emission, requires that upper levels warm slightly in compensation, leading to a slightly warmer moist adiabat. (Relative humidity in the upper troposphere of the convecting region increases because it is assumed by the model to vary in proportion to the surface value, which increases by roughly 3% in response to the reduction in surface radiation by dust.)

Thus, cooling at the surface of the convecting region is limited by the need to maintain the upper-tropospheric emitting temperature near its unperturbed value. This in turn requires that the surface temperature and moisture adjust so that the moist adiabat arising from the boundary layer is nearly unchanged. Despite the decrease in surface evaporation, surface specific humidity in the convecting region increases slightly (Fig. 4b), as a result of the reduced subsidence that flushes the boundary layer with dry upper-tropospheric air [e.g., Eq. (A7)], and the surface temperature decreases slightly in compensation. (The reduction of subsidence by dust is discussed below.)

The dependence of OLR upon emitter concentration suggests that the response to dust radiative forcing may depend upon the perturbation in upper-tropospheric moisture and how this is calculated by our model. We currently assume that as the surface relative humidity increases, deep convection will moisten the upper troposphere in response, as suggested by the analysis of observed tropical variations in relative humidity by Sun and Oort (1995). As a sensitivity study, we calculate the model response assuming that upper-tropospheric moisture in the convecting region is unperturbed by dust forcing. The absence of upper-level moistening allows the upper-tropospheric temperature to remain roughly unchanged, along with the moist adiabat of the convecting region (not shown). Since the surface specific humidity increases by roughly the same amount as before, the smaller perturbation to the moist adiabat causes the surface temperature to decrease by an additional 0.1 K. Conversely, a 3% increase in upper-tropospheric relative humidity in the first case causes the perturbed surface temperature in the convecting region to increase by 0.1 K.

The trivial perturbation by soil dust to the net radiative gain at the top of the dust layer is also fundamental to the response at the surface of the nonconvecting region. Because this gain is nearly unchanged, the import of moist static energy from the convecting region into the nonconvecting region must also remain unperturbed, as demonstrated by Fig. 4h and the perturbed version of (4):

$$a_c R_c'(z_T) = -[a_c M_c(\overline{h}_{B,w} - \overline{h}_{B,c})]'$$
$$= -a_c M_c'(\overline{h}_{B,w} - \overline{h}_{B,c}) - a_c \overline{M}_c(h_{B,w}' - h_{B,c}'), \quad (9)$$

where we have assumed for simplicity that ocean dynamical and atmospheric eddy transports to midlatitudes are unchanged by the dust. Now M_c, the rate of subsidence within the nonconvecting branch, is approximately proportional to radiative cooling [cf. (A6)]. Ra-

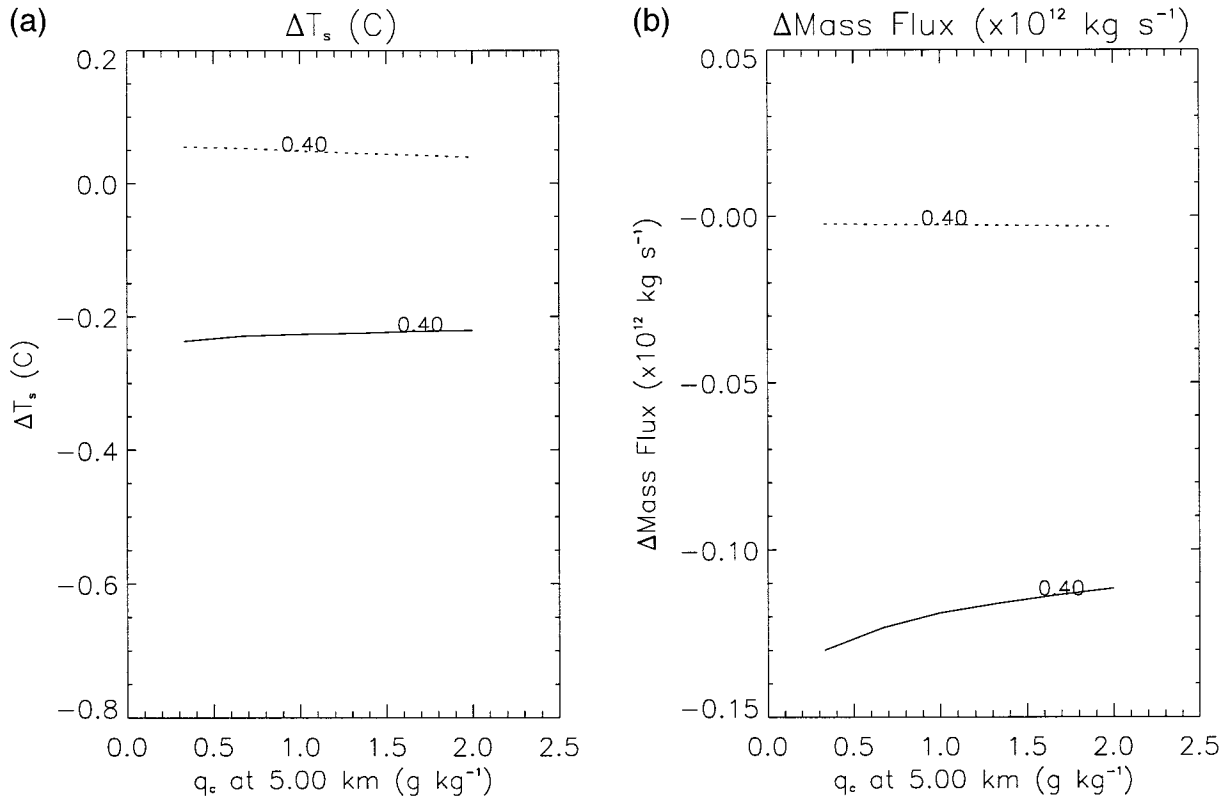

FIG. 5. Same as Fig. 4 but with dust radiative forcing applied only to the convecting region.

diative heating within the dust layer offsets this cooling rate through the absorption of sunlight, reducing M_c, as shown in Fig. 4f. Thus, even though the export of moist static energy into the nonconvecting region is nearly unchanged, the strength of the circulation is reduced, requiring that $h'_{B,w} - h'_{B,c}$, the difference in moist static energy between the two regions, increase in compensation. Comparison of Figs. 4e and 4g shows that $h_{B,c}$ must decrease, requiring some combination of cooling and drying at the surface of the nonconvecting region. In fact, both happen, as illustrated by Figs. 4a and 4b. The weakened subsidence caused by dust radiative forcing also accounts for the reduced advection of dry upper-tropospheric air into the boundary layer, allowing the relative humidity to increase, despite the reduced evaporation.

In summary, the large reduction in surface radiation by dust aerosols need not lead to cooling at the surface. In fact, substantial cooling at the surface of the convecting region is prohibited by the trivial perturbation by dust to the radiative flux at the top of the dust layer. This requires that the upper-tropospheric temperature remain nearly unchanged, which constrains the surface change to be correspondingly small, since these levels are related by the same moist adiabat. Cooling can occur within the nonconvecting region, as depicted in Fig. 4a, although this is not a consequence of the reduced surface radiation by itself, but rather the reduced *difference* between the surface and tropopause radiative perturbations, which corresponds to reduced radiative cooling of the troposphere. As a result of this diminished cooling rate, the subsidence rate is reduced, requiring an increased gradient of moist static energy to maintain the energy export from the convecting region at its unperturbed value. Cooling at the surface of the nonconvecting region relative to the convecting region occurs in order to increase this gradient. This behavior suggests why, in the AGCM experiments of Miller and Tegen (1998), cooling over the Arabian Sea is greater during the NH winter, even though the dust concentration overhead is substantially less than the summertime value. During NH summer, deep convection is frequent over the Arabian Sea in association with the Asian monsoon. In contrast, the ITCZ moves southward across the equator in the winter, so that the Arabian Sea underlies the nonconvecting branch of the circulation.

We next confine the dust radiative forcing to a single region and examine whether the response is limited to the region of the forcing or else induces a perturbation in the adjacent region. First, we consider the case of forcing confined to the convecting region. The change in surface temperature is shown in Fig. 5a. The response within the convecting region is nearly identical to that when dust is spread uniformly over both regions. However, surface temperature (and all other fields) within the nonconvecting region is approximately unchanged.

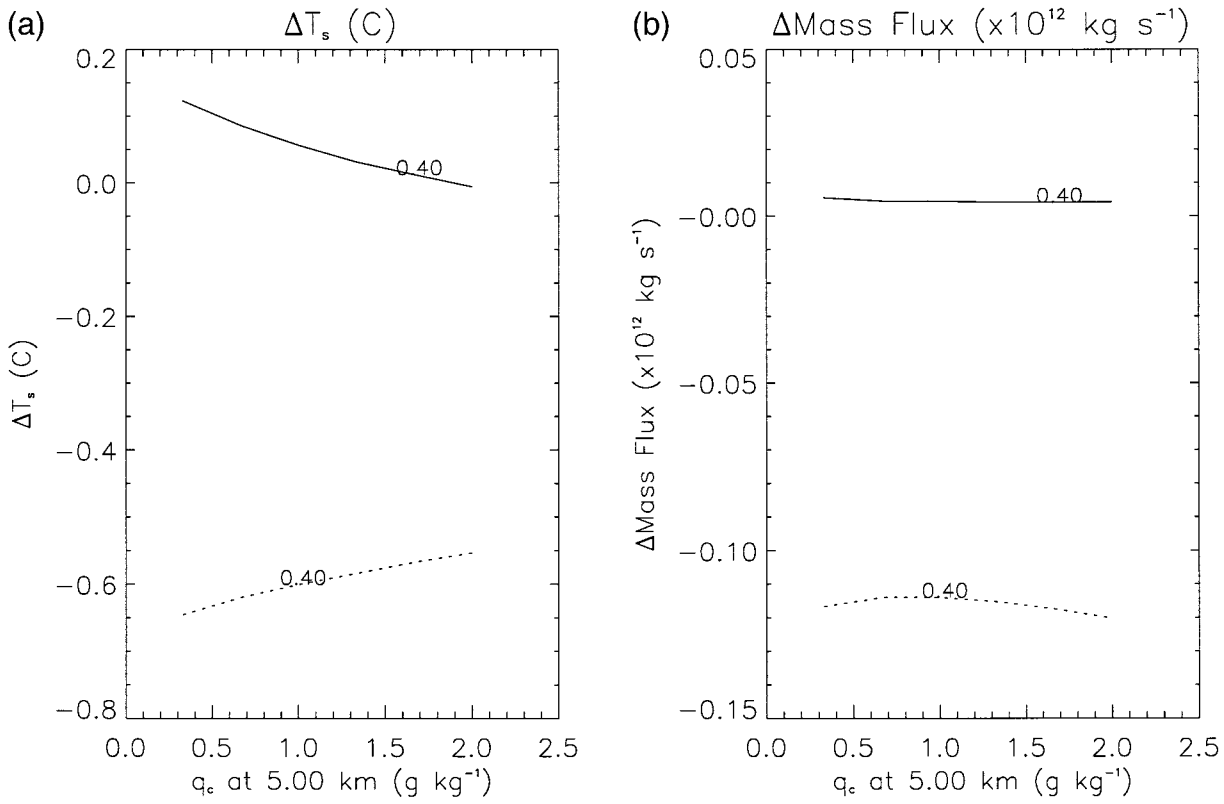

FIG. 6. Same as Fig. 4 but with dust radiative forcing applied only to the nonconvecting region.

As before, the large reduction in surface radiation is balanced by a decrease in the evaporative flux, caused mainly by an increase in relative humidity along with a decrease in the air–sea temperature difference, rather than through cooling of the surface. Temperature at the surface of the convecting region is constrained, as noted above, by the need to maintain the unperturbed value of outgoing longwave radiation, which depends upon the upper-tropospheric temperature and thus the surface value, as a result of convective mixing.

Figure 5b shows that M_c, the strength of the circulation linking the two regions, remains unchanged by dust. This might appear surprising at first, because dust radiative forcing augments the diabatic heating within the updrafts, which by itself would increase the average rate of ascent within the convecting region (equal to M_c). However, while the radiative heating rate is increased through the absorption of sunlight by dust particles, the intercepted radiation results in a reduction of the flux incident upon the surface. As noted above, the decrease in the surface flux is largely balanced by a decrease in surface evaporation, which reduces the latent heat release within the updraft. Because the anomalous net flux at TOA is nearly zero, the increase in atmospheric radiative heating by dust is almost precisely canceled by the reduction of the surface flux and the corresponding decrease in latent heat release, resulting in a circulation whose strength is unchanged, as shown in Fig. 5b. Our interpretation of the small change in convecting region surface temperature and circulation strength M_c, despite the large reduction in surface forcing, is analogous to the argument made by Pierrehumbert (1995) as a critique of the cirrus thermostat hypothesis (Ramanathan and Collins 1991). Both deep convective clouds and dust aerosols reduce the net radiative flux at the surface while leaving the net flux at cloud top nearly unperturbed (e.g., Kiehl 1994).

For the case of dust confined to the nonconvecting region, the perturbation to surface temperature is shown in Fig. 6a. This time, the response within the convecting region is negligible, and cooling within the nonconvecting region is nearly identical to the case of forcing in both regions. This might suggest that each region can respond locally to dust forcing without disturbing the adjacent region. However, for the reason described above, surface cooling by dust results from the weakened mass exchange within the convecting region (Fig. 6b) and the need to maintain the unperturbed import of moist static energy into the nonconvecting branch. Furthermore, in the next section, we show that dust confined to either region is able to perturb the climate in both regions, so long as the radiative forcing at the top of the dust layer is nonzero.

Because dust concentrations are largest over land (e.g., Tegen and Fung 1994, 1995), we recomputed the response of a direct circulation to dust radiative forcing,

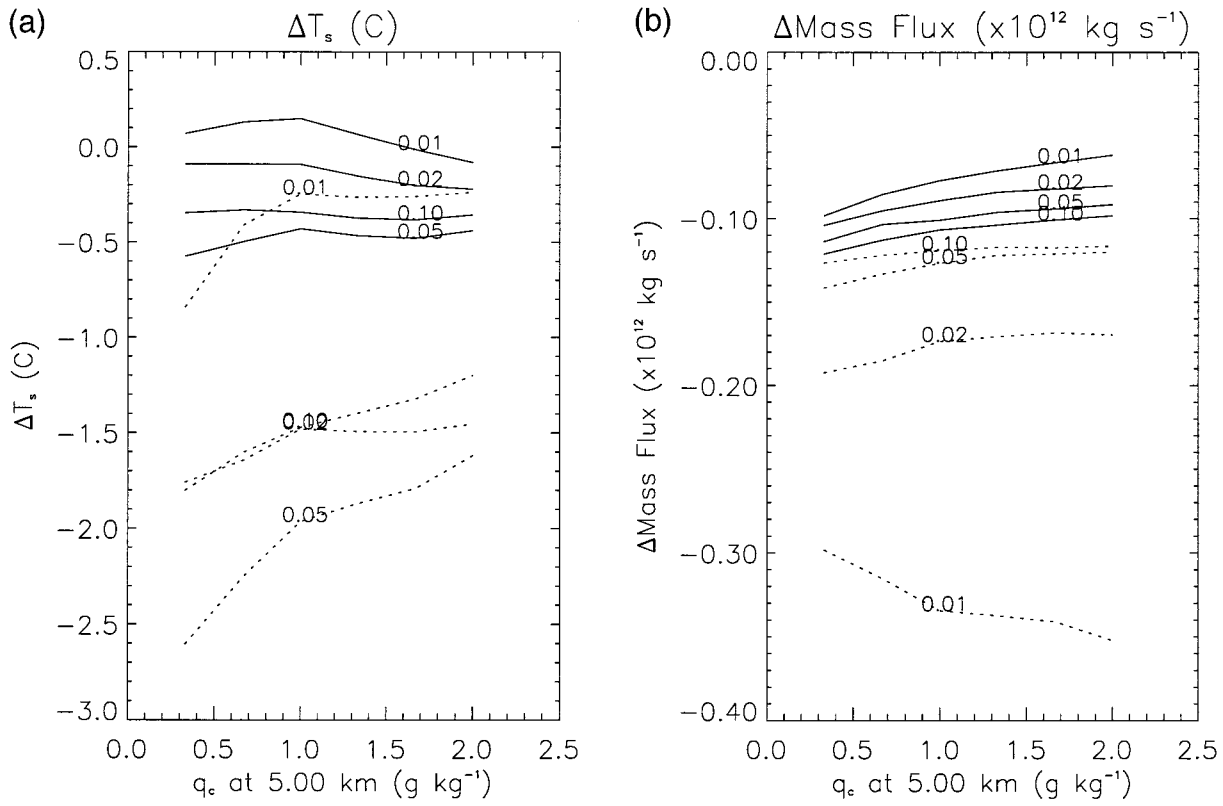

FIG. 7. Same as Fig. 4 but with dust radiative forcing applied to a continental direct circulation. Each curve corresponds to a different value of β_c, the evaporation efficiency of the nonconvecting region.

assuming that the circulation lies above a land surface. The response of surface temperature to a reduction of 30 W m^{-2} in the net radiative flux at the surface of both regions is shown in Fig. 7a. Except for the driest conditions ($\beta_c = 0.01$), cooling in the nonconvecting region is roughly twice as large compared to the oceanic case (cf. Fig. 4a). Part of this difference can be accounted for by referring to the perturbed difference in moist static energy between the two regions [cf. Eq. (9)]:

$$h'_{B,w} - h'_{B,c} = C_P(T'_{s,w} - T'_{s,c}) + L(q'_{B,w} - q'_{B,c})$$
$$\approx \left(C_P + L\overline{r}_w\frac{dq^*}{dT}\right)T'_{s,w} - \left(C_P + L\overline{r}_c\frac{dq^*}{dT}\right)T'_{s,c}, \quad (10)$$

where the neglected terms are proportional to the relative humidity perturbation in each region. For both the continental and oceanic cases, the perturbation to the moist static energy difference is roughly the same, reflecting similar weakening of the circulation by dust radiative heating (Fig. 7b). Because relative humidity (r_c) in the continental case is roughly half the oceanic value, the perturbed contrast in moist static energy between the two regions is manifested to a greater extent as a difference in temperature rather than humidity, thus accounting for the larger cooling in the nonconvecting region.

Cloud radiative forcing is held fixed in these experiments, as described in the appendix. Because deep convective clouds have a negligible effect upon the net radiation at the top of the atmosphere and do not perturb the radiative cooling within the nonconvecting region (and thus the mass exchange between the two regions), the sensitivity of our model to convective cloud forcing is small and approximately given by Fig. 5, if the radiative forcing is attributed to convective clouds rather than dust. In contrast, low clouds can change the radiation entering the troposphere, because their ability to reflect sunlight dominates their ability to trap longwave radiation originating at the surface. The parameterization of low cloud cover is an open question. Over the oceans, low cloud cover is related empirically to low-level static stability (Klein and Hartmann 1993), defined as the difference in potential temperature between the surface and some level just above the trade inversion. Because of the prohibition of horizontal temperature contrasts above the boundary layer, potential temperature above the trade inversion is related to the moist adiabat arising from the boundary layer of the convecting region (Miller 1997). Thus, the low-level static stability of this model should depend upon the differ-

ence in surface temperature between the convecting and nonconvecting regions. Because cooling by dust aerosols is greater at the surface of the nonconvecting region, static stability and thus low cloud cover should increase, which would result in further cooling. While oceanic low clouds are better related to static stability than relative humidity (Slingo 1980), this distinction may not hold for low clouds over land. In any case, we note that radiative forcing by dust increases the relative humidity of the surface layer in both regions (e.g., Fig. 4d). Were low cloud cover to increase, additional cooling would occur, indicating a positive feedback. We note that the direction of this feedback is not settled. Hansen et al. (1997) find that heating by an aerosol layer within an AGCM typically increases the temperature and lowers the relative humidity and cloud cover, which they refer to as the ''semi-indirect'' effect of aerosol forcing. Aerosol forcing in the latter study is confined to a single model layer and presumably does not alter the subsidence rate over a large vertical extent, so that the heating is instead balanced by an increased layer temperature. The contrasting behavior of our model suggests that the semi-indirect effect is not universal and depends upon the precise form of the aerosol forcing, including its magnitude and vertical extent, which determine the reduction in subsidence and entrainment of dry air into the boundary layer.

4. Sensitivity experiments

The experiments in the previous section show that radiative forcing by dust aerosols at the top of the dust layer is a strong constraint upon the climate response, and in particular upon surface temperature, overwhelming the comparatively large forcing at the surface. The radiative forcing attributed to dust in these experiments was chosen to resemble the forcing in the AGCM experiments of Miller and Tegen (1998). Despite the large range of optical properties exhibited by dust particles (e.g., Sokolik and Toon 1996), the AGCM assumes a uniform particle composition. In fact, the mineral composition and thus the optical properties of dust will vary with the source region of the particles, so that the observed TOA forcing should have regional variations. This suggests that the climate response will vary regionally with the composition of the dust particles. In this section, we perturb the optical properties of soil dust and recalculate the climate response. We also consider the effect of reducing the height of the dust layer, which was assumed in the previous section to extend to the tropopause. Recent modeling results (Tegen and Miller 1998) suggest that this overestimates the vertical extent of tropospheric dust, although this is a poorly observed quantity, especially in the Tropics.

A relatively simple way to perturb the optical properties of aerosol particles is through the single-scattering albedo $\tilde{\omega}_0$. Because the extinction optical thickness, which measures the attenuation of the beam due to the combined effects of aerosol scattering and absorption, is not changed (so that the energy lost by the beam during each scattering event is held constant), an increase in the single-scattering albedo corresponds to greater scattering and reduced absorption, and vice versa. Following Hansen et al. (1997), $\tilde{\omega}_0$ is changed uniformly at all wavelengths. We consider two cases corresponding to either a 10% increase or else a 10% decrease in the single-scattering albedo. (The increase in the single-scattering albedo is carried out subject to the constraint that $\tilde{\omega}_0$ be no greater than unity for any wavelength.) Given this change, we recompute the dust radiative forcing, using an estimate of the dust concentration derived from an offline chemical tracer model, as described in Tegen and Fung (1994, 1995). The global average of the forcing is listed in Table 1. Of relevance to our tropical model is the net forcing at the surface and top of the dust layer. A 10% increase in $\tilde{\omega}_0$, corresponding to reduced absorption, causes a reduction of radiation gained at the top of the column, so that the effect of soil dust more closely resembles forcing by sulfate aerosols. The greater reflectivity of the particles reduces the atmospheric radiative heating, as evidenced by the closer agreement of the TOA and surface forcing. In contrast, when $\tilde{\omega}_0$ is decreased by 10%, the greater absorptivity of the particles causes a gain in the energy absorbed at the top of the column and greater radiative heating. The sensitivity of the forcing, which is disproportionate in comparison to the 10% change in single-scattering albedo, reflects the fact that a beam of sunlight can scatter many times within the dust cloud before reaching the surface. According to the net TOA flux listed in Table 1, the value of $\tilde{\omega}_0$ used in the AGCM experiments is poised between trapping more energy within the column and expelling more through reflection. While this value, near 0.9, is within the range of observed single-scattering albedos given by Sokolik and

TABLE 1. Global-average radiative forcing by mineral dust aerosols as a function of the single-scattering albedo $\tilde{\omega}_0$. The middle column (labeled $1.0 \times \tilde{\omega}_0$) represents our current estimate of the dust forcing. In the remaining columns radiative forcing is recomputed, assuming that the single-scattering albedo is 10% smaller or larger. [The values in the center column differ slightly from those listed in Table 2 of Miller and Tegen (1998), because a different dust concentration is assumed in the two calculations.]

Jun–Aug global-average anomaly (W m^{-2})	$0.9 \times \tilde{\omega}_0$	$1.0 \times \tilde{\omega}_0$	$1.1 \times \tilde{\omega}_0$
Surface flux			
Solar	−4.53	−3.17	−2.18
Thermal	0.25	0.25	0.25
Net	−4.28	−2.92	−1.93
TOA flux			
Solar	1.15	−0.45	−1.57
Thermal	0.47	0.47	0.47
Net	1.62	0.02	−1.10
Net radiative heating	5.90	2.94	0.83

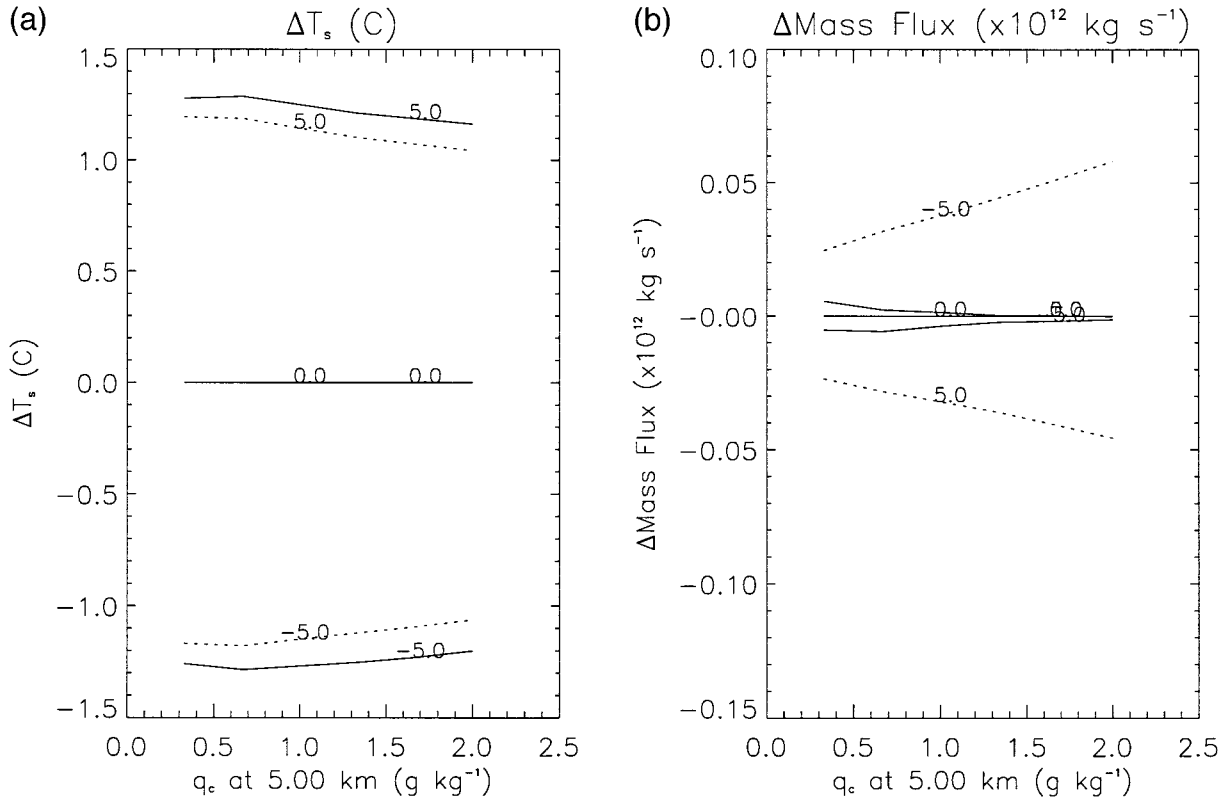

FIG. 8. Perturbation to the solutions for the convecting (solid) and nonconvecting (dashed) regions of an oceanic direct circulation by radiative forcing corresponding to −5, 0, and 5 W m^{-2} at the surface and tropopause of both regions. (a) Surface temperature (°C); and (b) area-integrated mass fluxes, i.e., M_w and M_c times the area of the convecting and nonconvecting regions, respectively ($\times 10^{12}$ kg s^{-1}).

Toon (1996), our perturbation of 10% in either direction is also within the observed range.

Before applying this forcing to the model and measuring the sensitivity of the response to the changed dust absorptivity, we carry out an experiment where the net forcing at the top of the dust layer is varied (between −5 and 5 W m^{-2}) but the forcing within the atmosphere (i.e., the difference in forcing between the surface and top of the layer) is equal to zero. This is intended to complement the experiments of the previous section, where the model was forced by atmospheric radiative heating in the absence of a perturbation at the top of the dust cloud. The change in surface temperature for the different values of the net forcing at cloud top is shown in Fig 8a. Not surprisingly, both regions cool at the surface when the net flux into the column is decreased. The sensitivity is roughly 0.25 K/(W m^{-2}) of TOA forcing, similar to the AGCM sensitivity with respect to changes in solar forcing and CO_2 concentration (Hansen et al. 1997). The sensitivity of surface temperature is slightly greater in the convecting region due to the clear-sky water vapor feedback present in the model as a result of coupling upper-tropospheric humidity to the surface value in this region. Comparing Fig. 4a to Fig. 8a, it is apparent that the climate is much more sensitive to forcing at the top of the atmosphere compared to a perturbation applied at the surface.

While the similar response in each region might suggest that each region is adjusting locally to the radiative perturbation, this symmetry is in fact a consequence of the unperturbed atmospheric radiative heating, rather than a signature of local adjustment. If the radiative perturbation is applied only in the convecting region, then there is a similar (albeit smaller) change in temperature at the surface of the nonconvecting region, as shown in Fig. 9a. This is because the change in the TOA radiative gain in the convecting region perturbs the export of moist static energy to the nonconvecting region. Since the mass exchange between the two regions, proportional to the trivially perturbed atmospheric radiative heating, is unchanged (Fig. 9b), the difference in moist static energy between the two regions must adjust, leading to a change in temperature in the nonconvecting region, where direct forcing is absent.

We now calculate how the climate response varies with the absorptivity of the dust particles, characterized in terms of the single-scattering albedo $\tilde{\omega}_0$. Corresponding to $\tilde{\omega}_0$ equal to 0.9, 1.0, and 1.1 times the value used in the previous section, we set the perturbation to the net radiative flux at the top of the dust layer equal to

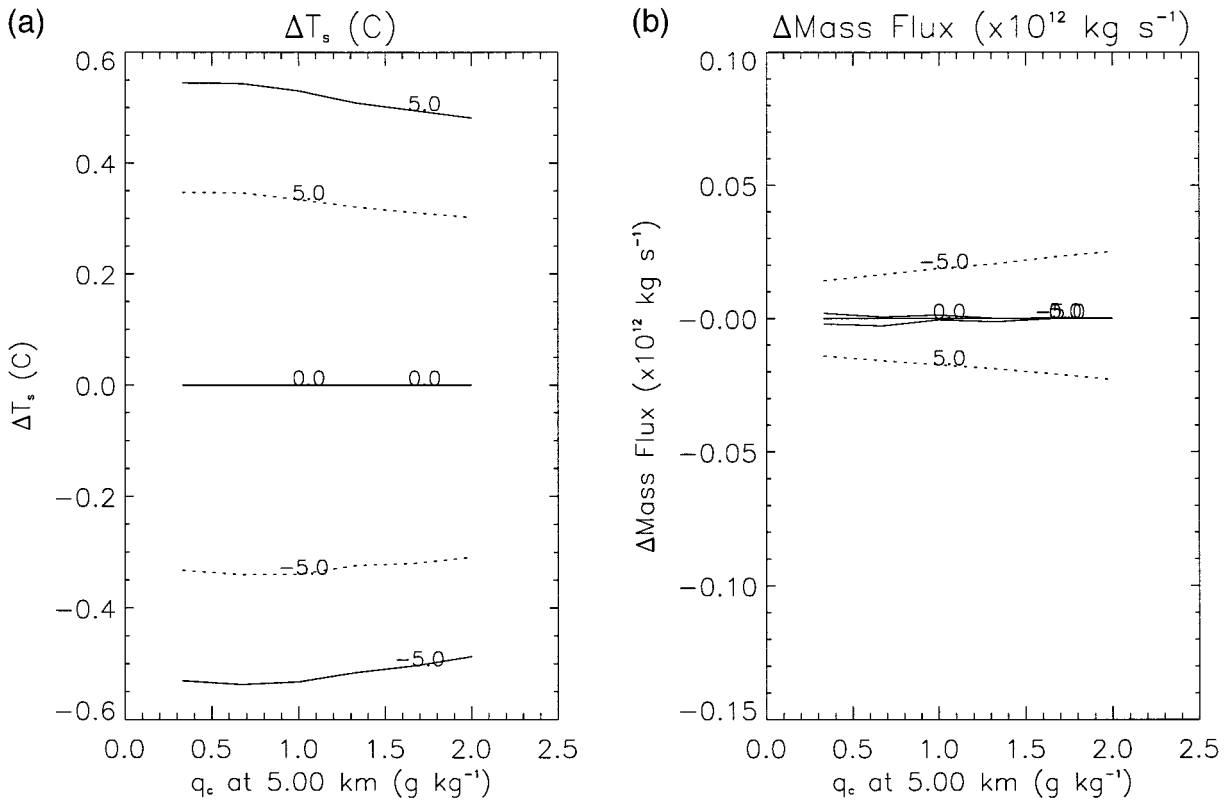

FIG. 9. Same as Fig. 8 but with radiative forcing applied only to the convecting region.

−5, 0, and 5 W m^{-2}, while the perturbation to the net radiation at the surface is set equal to −10, −15, and −20 W m^{-2}, respectively (cf. Table 2). This forcing is roughly in proportion to the globally averaged forcing listed in Table 1 and is comparable to the dust radiative forcing averaged over the extent of the dust cloud computed by the tracer model of Tegen and Fung (1994, 1995). If the dust particles are made more absorbing ($\tilde{\omega}_0 = 0.9$), then not only is there an increase in the TOA radiative gain, but also in the radiative heating within the dust layer.

The dependence of surface temperature upon the absorptivity of the dust particles is shown in Fig. 10a. As the particles become less absorbing ($\tilde{\omega}_0 = 1.1$), both regions cool. This cooling is a consequence of the TOA forcing, rather than the reduction of the net radiative flux at the surface. This is demonstrated by the warming of both regions in response to absorbing dust particles ($\tilde{\omega}_0 = 0.9$). This warming occurs even though the reduction in the surface flux is four times the increase at TOA. This again emphasizes that the TOA forcing has a much greater impact upon the response than the surface forcing. The latter perturbs the climate through its effect upon the atmospheric radiative heating rate, which depends upon the difference in forcing between the surface and the top of the dust layer. As this heating increases, the strength of the circulation decreases (Fig. 10b), requiring a larger difference in surface moist static energy between the two regions, which results in a larger difference in surface temperature, as illustrated by Fig. 10a.

We repeated these sensitivity experiments for the case of a continental direct circulation, with β_c set equal to 0.10. The dependence of surface temperature upon $\tilde{\omega}_0$ is shown in Fig. 11. The sensitivity of the continental circulation to changes only in the forcing at the top of the layer is approximately the same as for the oceanic case (not shown). However, from the previous section, we know that the continental circulation is more sensitive to changes in the atmospheric radiative heating rate. This is evident in Fig. 11, which shows that the asymmetry of the response between the convecting and nonconvecting regions is greater than for an oceanic circulation.

TABLE 2. Perturbation to the net radiative flux at the top and base of the dust layer for the calculation shown in Figs. 10 and 11, as a function of the single-scattering albedo of dust particles. Here $\tilde{\omega}_0$ is the unperturbed value of this parameter.

Net radiative perturbation (W m^{-2})	$0.9 \times \tilde{\omega}_0$	$1.0 \times \tilde{\omega}_0$	$1.1 \times \tilde{\omega}_0$
Base of dust layer	−20	−15	−10
Top of dust layer	5	0	−5
Net radiative heating	25	15	5

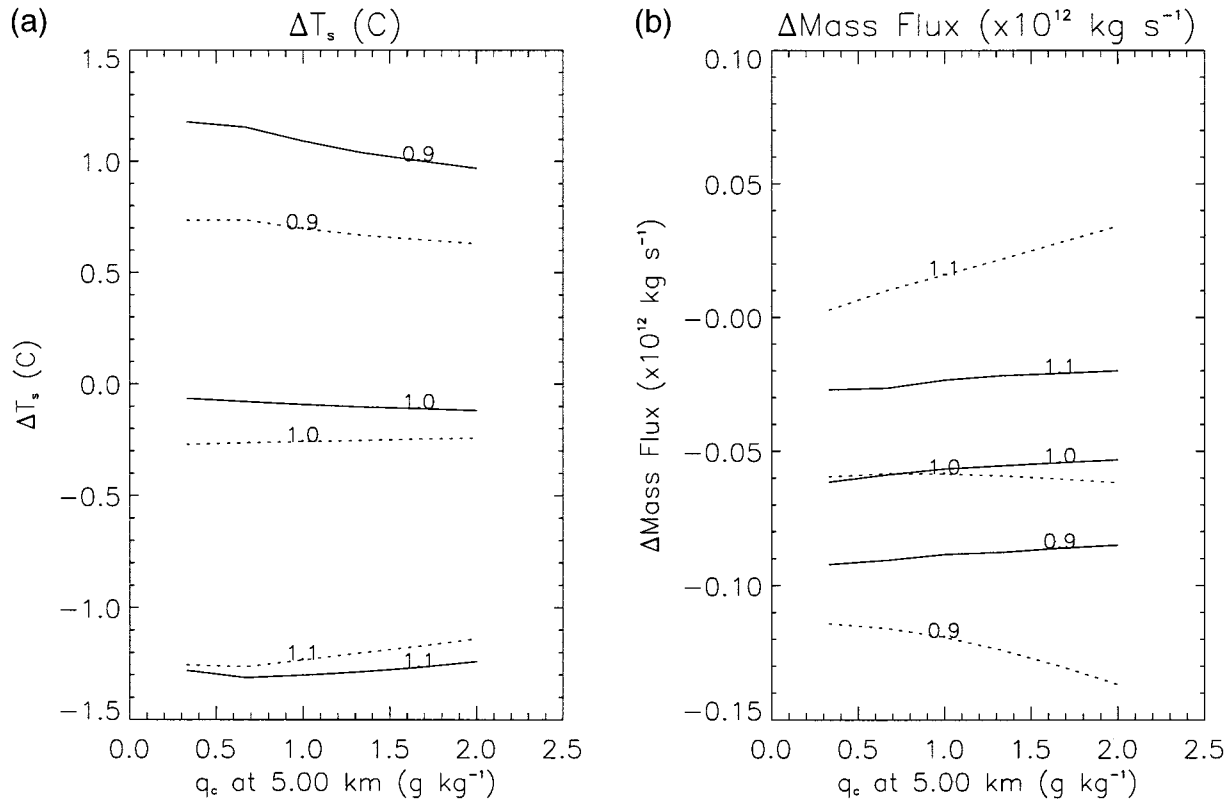

FIG. 10. Perturbation to the solutions for the convecting (solid) and nonconvecting (dashed) regions of an oceanic direct circulation by dust radiative forcing as a function of the single-scattering albedo $\tilde{\omega}_0$ of the dust particles. (The perturbations to the net radiative flux at the top and base of the dust layer are listed in Table 2.) (a) Surface temperature (°C); and (b) area-integrated mass fluxes, i.e., M_w and M_c times the area of the convecting and nonconvecting regions, respectively ($\times 10^{12}$ kg s^{-1}).

We have also calculated the sensitivity of our results to changes in the height of the dust layer. In the calculations so far, we have assumed that the dust layer extends to the tropopause. Observations of the vertical distribution of dust aerosols consist mainly of instantaneous profiles, with little information about the more diffuse distribution that exists on the timescale of weeks to months. Modeling studies (Tegen and Fung 1994, 1995) suggest that dust aerosols can be lofted quite high in the troposphere in regions of deep convection such as the Arabian Sea during NH summer, although improved versions of the model suggest that this vertical extent is possibly overestimated (Tegen and Miller 1998). As a sensitivity study, we set the forcing of net radiation at the surface to -30 W m^{-2}, and the perturbation at the top of the dust layer equal to zero as in the previous section. We then vary the top of the dust layer from the tropopause to 0.50 and 0.33 times this value. In addition, we consider a case where dust is confined to the boundary layer beneath the trade inversion. As in the previous section, the radiative heating by dust aerosols is assumed to be uniform with respect to pressure.

Figure 12a shows the change in temperature when an ocean underlies the circulation. As the top of the dust layer approaches the trade inversion, so that the dust radiative forcing is increasingly confined within the boundary layer, the perturbation to surface temperature falls to zero. However, the surface response is only weakly sensitive to the height of the dust cloud, so long as it extends above roughly one-third to one-half the depth of the troposphere.

The sensitivity to the height of the dust cloud can be understood by noting that the change in surface temperature within the nonconvecting region depends upon the reduction in the mass exchange with the convecting region. This exchange rate in turn depends upon the radiative heating within the dust layer, which offsets the clear-sky radiative cooling, as shown in (A6). As the dust layer becomes concentrated near the surface, more and more of this heating occurs in the well-mixed layer of uniform dry static energy near the surface, where radiative cooling is balanced by the surface sensible heat flux [cf. (A4)], rather than adiabatic warming. That is, the response of surface temperature to dust depends upon the ability of the dust cloud to reduce the radiative cooling above the boundary layer, where this can affect the strength of the circulation. Figure 12b shows that the perturbation to the subsidence rate within the nonconvecting branch falls to zero as the dust layer becomes

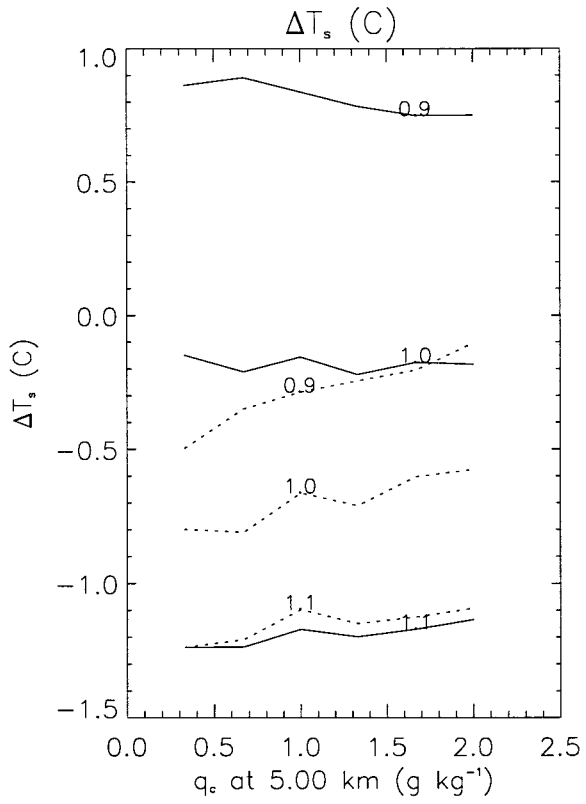

FIG. 11. Same as Fig. 10 but with dust radiative forcing applied to a continental direct circulation.

more confined within the boundary layer. Furthermore, the air–sea temperature difference increases as the extent of the dust layer decreases (Fig. 12c), a sign that the radiative heating within the dust layer is being increasingly balanced by the surface sensible heat flux [cf. Eqs. (1) and (A4)]. For this reason, the SST perturbation shows relatively little sensitivity to the extent of the dust cloud, since the reduced change in surface air temperature is offset by the increase in the air–sea temperature difference as the top of the dust cloud approaches the surface (Fig. 12d). In summary, a change of temperature at the surface beneath a dust cloud requires either that the cloud extend above the layer mixed by dry convection, or else that the radiative perturbation at the top of the cloud be nonzero so that the temperature at all levels can change. Furthermore, a dust cloud above the boundary layer has a larger effect upon surface temperature than the same dust concentration within the boundary layer.

We repeated the calculation for a continental direct circulation and found a similar sensitivity to the vertical extent of the dust layer (Fig. 13). For β_c equal to 0.10, the change in surface temperature is relatively insensitive to the height of the dust layer as long as the top of the layer extends a few kilometers above the surface. However, this sensitivity depends upon β_c. As β_c is decreased from 0.10 to 0.05, the height of the boundary layer in the absence of dust nearly doubles to just under 2 km (cf. Fig. 3j). As β_c is reduced, and the dry convective boundary layer expands with respect to height, the dust cloud must extend higher into the troposphere in order that a majority of the radiative heating can be offset by reduced adiabatic descent, rather than sensible heating within the isentropic boundary layer.

Note that for β_c equal to 0.10, the surface of the nonconvecting region actually warms slightly when the dust cloud is confined to within the boundary layer (Fig. 13). This may appear surprising at first, since the radiative forcing at the top of the dust cloud is zero by construction, and the surface forcing is strongly negative. However, were the surface temperature to remain unperturbed by dust, the decrease in the surface sensible heat flux, which compensates the reduced surface radiative flux, would necessitate a decrease in the ground temperature [cf. Eq. (A4)]. This cooling of the ground would reduce the net emission of longwave radiation by the surface, which would reduce the net upward emission at the top of the dust layer. To maintain the original net flux at this level, which is unperturbed by the dust particles, the boundary layer must heat up slightly, accounting for the warming shown in Fig. 13. In contrast, this warming is absent at the surface of the convecting region, and in both regions of the oceanic case (Fig. 12a), since the boundary layer is sufficiently moist that the upward longwave emission at the top of the boundary layer is roughly independent of the surface emission and temperature.

The diminishing perturbation of the surface temperature as the dust layer becomes more closely confined to the surface is analogous to the disproportionately small cooling at the surface of the convecting region that was found in the previous section. In that example, the dust cloud lies within a layer (i.e., the entire troposphere) well mixed by *moist* convection, and the trivial radiative forcing at the top of the dust layer obviates any large change at the surface.

5. Conclusions

We have examined the effect of radiative forcing by soil dust aerosols upon a simple model of a tropical

→

FIG. 12. Perturbation to the solutions for the convecting (solid) and nonconvecting (dashed) regions of an oceanic direct circulation by dust radiative forcing as a function of the height of the dust cloud. (a) Surface temperature (°C); (b) area-integrated mass fluxes, i.e., M_w and M_c times the area of the convecting and nonconvecting regions, respectively ($\times 10^{12}$ kg s^{-1}); (c) sea–air temperature difference (°C); and (d) SST (°C). Each curve is denoted by cloud height as a fraction of the tropopause height, with ''Inv'' denoting the case where the cloud top is at the top of the boundary layer.

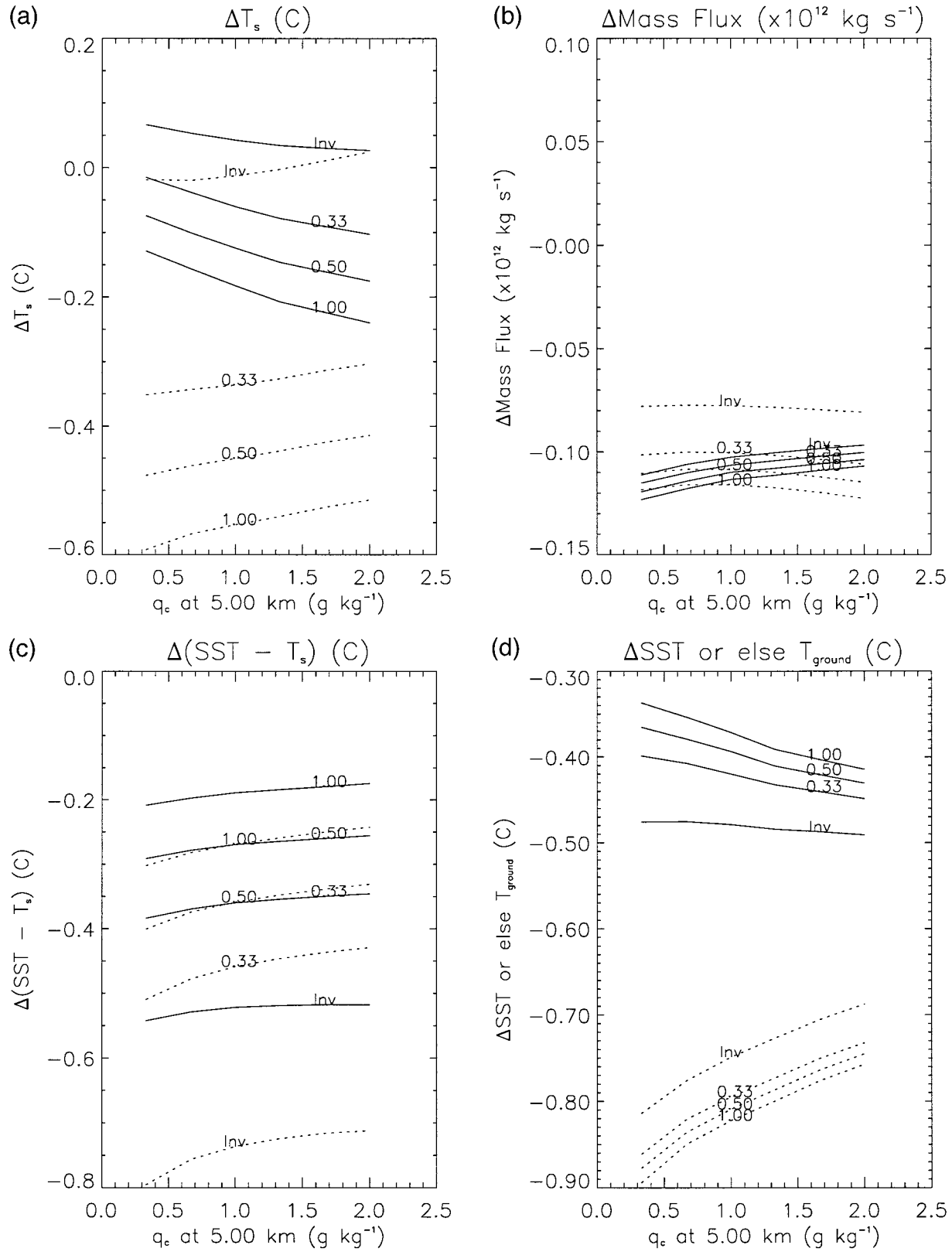
(a)
ΔT_s (C)
ΔT_s (C)
q_c at 5.00 km (g kg^-1)
Inv
Inv
0.33
0.50
1.00
0.33
0.50
1.00
(b)
ΔMass Flux (x10^12 kg s^-1)
ΔMass Flux (x10^12 kg s^-1)
q_c at 5.00 km (g kg^-1)
Inv
0.33
0.50
1.00
(c)
Δ(SST − T_s) (C)
Δ(SST − T_s) (C)
q_c at 5.00 km (g kg^-1)
1.00
1.00
0.50
0.50
0.33
0.33
Inv
Inv
(d)
ΔSST or else T_ground (C)
ΔSST or else T_ground (C)
q_c at 5.00 km (g kg^-1)
1.00
0.50
0.33
Inv
Inv
0.33
0.50
1.00

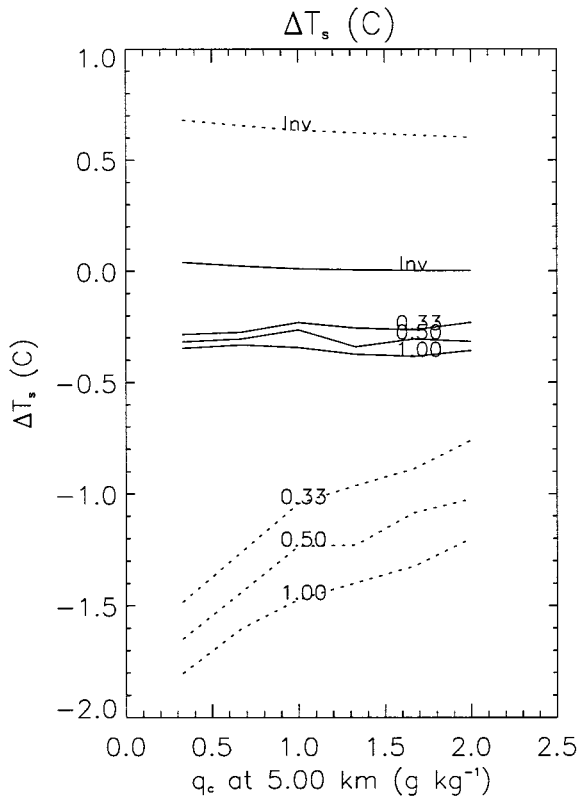

FIG. 13. Same as Fig. 12 but with dust radiative forcing applied to a continental direct circulation.

direct circulation. The model divides the Tropics into a region well mixed by deep convection and a nonconvecting region where air descends. The convecting region is further divided into isolated updrafts, with subsidence in between. For each region, budgets of dry static energy and moisture are constructed. In the limit of vanishing updraft area, an idealization motivated by the small observed fractional area of tropical deep convective clouds, moist static energy at the tropopause is equal to the value at the surface of the convecting region, as shown in Miller (1997). Dynamics is introduced implicitly, as in Pierrehumbert (1995), through the assumption that the large-scale circulation prohibits horizontal contrasts in temperature above the boundary layer.

Because dust aerosol concentrations are large over semiarid regions, which are the source of atmospheric dust, we consider the case of a direct circulation above a land surface in addition to an oceanic circulation. If the nonconvecting region is sufficiently dry, it can be several degrees warmer than the convecting region and still import energy, due to the augmentation of potential energy at the tropopause by the latent component (Fig. 3).

We perturb the model with radiative forcing attributed to soil dust aerosols. Dust aerosols absorb sunlight to a greater extent than sulfate aerosols, so that the net gain of radiative energy at the top of the dust layer is largely unchanged in comparison to the reduction of the net radiative flux at the surface. Thus, dust aerosols displace radiative heating at the surface into the dust layer, in contrast to sulfate aerosols, which being more reflective reduce the radiative gain of the atmospheric column and surface by similar amounts.

In our initial experiments, we idealize the radiative forcing at the top of the dust layer as zero, while reducing the surface flux by 30 W m^{-2}. The dust cloud is initially assumed to extend to the tropopause, as suggested by the distribution of dust estimated by Tegen and Fung (1994, 1995) for the Arabian Sea region during NH summer, where the dust radiative forcing is largest.

Within the convecting region, the change in surface temperature is nearly zero, despite the large reduction in the surface radiative flux. This flux anomaly is balanced by a reduction in the evaporation, which results mainly from an increase in the surface relative humidity and a decrease in the air–sea temperature difference, rather than from a reduction in surface temperature. The latter is prevented by deep convective mixing, which relates the surface temperature to the upper-tropospheric value by maintaining a moist-adiabatic lapse rate. The upper-tropospheric temperature is, in turn, constrained near its unperturbed value by the trivial radiative forcing at the top of the atmosphere, which requires that longwave radiation to space, a function of the upper-tropospheric temperature, remain unchanged (Cess et al. 1985). In principle, a reduction in surface temperature and longwave emission could occur if the energy export from the convecting region increased and this energy was emitted by the surrounding regions. However, this emission requires an increase in the upper-tropospheric temperature of the surrounding region, which is prohibited by the large-scale circulation that causes temperature across the extent of the circulation to vary in unison. Thus, the argument of Cess et al. (1985), which neglects changes in dynamical transports, can be extended to the convecting region of a tropical circulation, because a change in surface temperature inconsistent with the TOA radiative forcing cannot be compensated by anomalous OLR within the surrounding nonconvecting regions.

Larger cooling occurs at the surface of the nonconvecting region. However, the magnitude of this cooling is determined not by the reduction in surface radiation per se, but by the anomalous atmosphere heating associated with the absorption of radiation within the dust layer, which is the difference in forcing between the surface and top of the dust layer. This is because the export of moist static energy into the nonconvecting region must remain close to its original value, due to the negligible perturbation by dust to the net radiative flux at the top of the atmosphere. This export is proportional to the strength of the circulation linking the convecting and nonconvecting regions, and the differ-

ence in moist static energy at the surface of the two regions. Because subsidence in the nonconvecting region balances radiative cooling, the circulation is weakened by radiative heating within the dust layer. Consequently, the contrast in moist static energy between the two regions must increase, which necessitates greater cooling at the surface of the nonconvecting region. Because dust uplift from the surface depends upon the surface wind speed, the reduction in circulation strength by soil dust has the potential to feed back upon the atmospheric dust concentration. In a future article, we show that an AGCM experiment including dust radiative heating has a lower dust concentration, in comparison to an experiment where dust has no radiative effect.

The disproportionately small change at the surface of the convecting region resembles the negligible cooling over the Arabian Sea during NH summer, in the AGCM experiments of Miller and Tegen (1998). Cooling is absent in this region despite the large 60 W m^{-2} reduction in surface radiation during this season. Cooling does occur within this region during NH winter, in the presence of much smaller radiative forcing by dust. Our model suggests that this behavior is a result of the presence of convection associated with the ITCZ during NH summer.

Radiative forcing by clouds is held fixed in this model. In contrast, Hansen et al. (1997) note what they refer to as the semi-indirect effect, where cloud cover in an AGCM decreases in response to a decrease in relative humidity that accompanies radiative heating within the aerosol layer. In our model, relative humidity actually *increases* in response to dust forcing. This is a result of the reduced subsidence that otherwise flushes the boundary layer with dry upper-tropospheric air. We suggest that the existence of the semi-indirect effect should depend upon the magnitude of radiative heating within the aerosol layer, along with the depth over which this heating occurs, both of which control the anomalous advection of dry air from aloft into the boundary layer.

The small temperature change at the surface of the convecting region is a consequence of deep convective mixing that maintains a moist-adiabatic lapse rate. For very large radiative forcing by dust aerosols, and very large reductions in surface radiation, the convective circulation may not be sustainable, as in extreme nuclear winter calculations (e.g., Cess et al. 1985; Ghan et al. 1988). However, ''natural'' dust concentrations used to force an AGCM circulation have little effect upon the tropical lapse rate (Miller and Tegen 1998).

The importance of radiative forcing at the top of the atmosphere to climate at the surface has also been noted by Pierrehumbert (1995), with regard to tropical convective clouds. Deep convective clouds and dust aerosols reduce the net radiative flux at the surface by a similar magnitude, while leaving the net flux at the top of the cloud or dust layer nearly unperturbed (Chou 1994). In fact, one could alternatively regard the response of our model in Fig. 5 as the perturbation resulting from an increase in tropical convection. The model could also be applied to infer the climate effect of anomalous shortwave absorption (Cess et al. 1995; Ramanathan et al. 1995). If current radiation models underestimate the true atmospheric heating, then the main effect of a correction would be to weaken the rate of subsidence, while having only a small effect upon temperature at the surface and horizontal energy transport by the tropical circulation.

Energy transports to midlatitudes by atmospheric eddies and ocean currents are assumed to be unperturbed by aerosol forcing. We are currently investigating whether the ocean responds locally to surface radiative forcing—for example, through reduced evaporation—or through a perturbation in dynamical transports. As noted by Miller and Tegen (1998), this has implications for the atmospheric moisture budget and the precipitation anomaly resulting from dust.

The trivial forcing at the top of the atmosphere, which is fundamental to the response of our model, depends upon the optical properties of the dust particles. For simplicity, the particle index of refraction in the AGCM experiments of Miller and Tegen (1998) is assigned a single value derived from far-traveled Saharan dust, which is characterized by small TOA forcing. In reality, dust particles exhibit a wide range of optical properties that vary with the mineral composition of the source region. For example, Sahelian dust arriving at Barbados during the NH winter is darker than the reddish-brown summertime dust that originates on the fringes of the Sahara (Carlson and Prospero 1972). To estimate the sensitivity of our results to the dust optical properties, we increased or else decreased the single-scattering albedo $\tilde{\omega}_0$ of dust particles by 10% and recalculated the response. Sokolik and Toon (1996) find that this is a realistic range, given that our original value of $\tilde{\omega}_0$ is near 0.9. As the dust particles become more absorbing (corresponding to a decrease in $\tilde{\omega}_0$), the surface flux is reduced, but the radiation gain by the column increases. Table 1 shows that the sensitivity of the dust radiative forcing to this change is quite large. This sensitivity, proportionately greater than the 10% change in the single-scattering albedo, results from the fact that a beam of sunlight scatters many times before reaching the surface.

Experiments in which only the TOA forcing is varied, with the perturbation to the atmospheric radiative heating set equal to zero, show that the response of surface temperature is much more sensitive to the forcing at the top of the dust layer than the surface value. When forcing of the atmospheric radiative heating is included in the model, its effect is mainly to introduce an asymmetry in the response between the convecting and nonconvecting regions. For greater values of heating within the dust layer, temperature at the surface of the nonconvecting region is reduced in comparison to the convecting region value. The asymmetry of the surface temperature anomaly, which depends upon the perturbation

to the meridional circulation, will also depend upon the latitude of the convecting and nonconvecting regions (Lindzen and Hou 1988). These are fixed in this model, but could change depending upon the meridional distribution of dust radiative forcing at TOA.

The negligible radiative perturbation to the TOA radiative flux by dust particles in the AGCM experiments of Miller and Tegen (1998), along with the sensitivity of the response of our simple model to forcing at this level, suggest that the temperature change attributed to dust could be much larger if the optical properties of the aerosol particles were not assumed to be uniform and were allowed to vary with the mineral composition of the source region. The forcing associated with the optical properties currently assumed by the AGCM is poised between warming and cooling of the surface (cf. Fig. 10a). If the TOA forcing associated with a particular source region departs from zero, then the regional change in climate could be much larger than our current AGCM estimate. Accurate estimation of the regional change is important in order to distinguish the response forced by increasing concentrations of CO_2. While it may be impractical to model the entire observed range of dust optical properties, variations in mineral composition of the source region averaged over the scale of the direct circulation should at least be considered. This may require measurements of optical properties from a wider variety of mineral types over a broader range of wavelengths.

While satellite retrievals are providing increasingly accurate measurements of the horizontal distribution of dust aerosols (e.g., Husar et al. 1997; Moulin et al. 1997; Herman et al. 1997), little remains known about the vertical distribution of dust on timescales of weeks or more. We find that our model is relatively insensitive to the vertical extent of the dust cloud, so long as the layer extends significantly above the boundary layer. Within the boundary layer, radiative forcing by dust has little effect upon surface temperature since heating within the dust layer is balanced by the surface sensible heat flux rather than adiabatic descent. While a reduction of descent requires an increase in the surface moist static energy contrast between the two regions of the model, and a cooling of the nonconvecting region compared to the convecting region, a perturbation to the surface sensible heat flux can result simply by decreasing the air–ground temperature difference, leaving the surface temperature relatively unchanged. For oceanic regions, the climate response is insensitive to the depth of the dust layer, so long as the top of the layer extends above one-third to one-half the depth of the tropopause. Over arid land surfaces, where the boundary layer mixed by dry convection may extend higher above the surface, the dust cloud must extend correspondingly higher to have any effect. Lidar measurements extending over a few weeks or more can reduce some of the uncertainty regarding the vertical extent of dust aerosols on seasonal timescales.

The response of the tropical climate to radiative forcing by soil dust aerosols is sensitive to the assumed optical properties of the dust particles, along with their vertical distribution, and it is hoped that future measurements will be undertaken to reduce the uncertainty of this forcing.

Acknowledgments. We thank Amy Clement, Greg Hartke, Steve Klein, Kristin Larson, and Richard Seager for helpful conversations about the tropical circulation. Brian Cairns and Andy Lacis explained the radiative effect of dust aerosols and their parameterization in the NASA/GISS radiation model. We also benefited from discussions about dust aerosols with Phil Austin, Lionel Pandolfo, and David Tashima, along with Leo Donner and Anthony Slingo, the latter of whom suggested the importance of the depth of the dust layer. The article was improved by the comments of three anonymous reviewers. We are especially grateful to Inez Fung for scientific advice and suggestions about the organization of this work.

We thank the Climate Dynamics Program of the National Science Foundation for supporting this study through Grant ATM-94-22631.

APPENDIX

Model Equations

Here, we list the equations that compose our simple model of a tropical direct circulation. The model, described in general terms in section 2 and in detail by Miller (1997), divides the Tropics into a convecting region and a nonconvecting region where descent occurs. The convecting region is further divided into isolated updrafts, meant to represent cloud clusters, and a broad region of subsidence occurring between the updrafts. This arrangement is illustrated in Fig. 1, where variables representing the updraft, subsiding fraction of the convecting region, and nonconvecting region are denoted by the subscripts u, w, and c, respectively. Budgets of dry static energy $s = C_pT + gz$ (in J kg^{-1}), and specific humidity q (in grams of vapor per kilogram of air), are constructed for the boundary layer and free troposphere of each region. In the upper layer, we also consider the mixing ratio l of liquid water and ice (referred to collectively as hydrometeors, in grams of water per kilogram of air).

The model can be simplified by assuming that the fractional area of the updraft region, a_u, is vanishingly small, an idealization motivated by Riehl and Malkus (1958), who observed that most tropical convection takes place within isolated ''hot towers,'' and by the small tropically averaged deep convective cloud cover diagnosed by ISCCP (cf. Miller 1997). In this limit, the moist static energy at the tropopause is equal to the surface value of the convecting region:

$$s_T + Lq_{T,u} = s_{B,w} + Lq_{B,w}$$
$$h_T = h_{B,w}, \tag{A1}$$

where $h = s + Lq$ is the moist static energy, and the subscripts T and B denote the tropopause and surface values, respectively.

Despite the vanishing of a_u, the total upward mass flux a_uM_u (in kilograms per second when multiplied by the area of the Tropics) remains nonzero and can be diagnosed from the continuity equation:

$$a_uM_u = a_wM_w + a_cM_c. \tag{A2}$$

Here, a_w and a_c are the fractional areas of the convecting region outside of the updrafts and the nonconvecting region, respectively, whose sum together with a_u is equal to unity. Ascent within the updraft region corresponds to a positive value of M_u, while M_w and M_c, the vertical mass flux throughout the remainder of the convecting region and the nonconvecting region, respectively, are defined to be positive downward. The vertical mass flux within each region is assumed to be uniform between the tropopause and z_B, the lifting condensation level, while decreasing to zero at the surface. Thus, detrainment from the updraft occurs within a vanishingly thin layer at the tropopause, with return flow, representing the trade winds, beneath the lifting condensation level.

a. Dry static energy budget

Between the surface and lifting condensation level of each region, a dry static energy budget can be constructed:

$$a_wM_w(s_{B,w} - s_{B^+,w}) + a_cM_c(s_{B,w} - s_{B,c}) = a_w[R_w(z_B) - R_w(0) + S_w] \tag{A3}$$

$$a_cM_c(s_{B,c} - s_{B^+,c}) = a_c[R_c(z_B) - R_c(0) + S_c], \tag{A4}$$

where S is the surface sensible heat flux and R is the net radiative flux (positive downward), both in watts per meter squared. The subscript B^+ denotes the dry static energy just above the top of the layer at z_B. We assume that dry static energy is continuous across this boundary, neglecting the small inversion formed by dry convective mixing that is typically less than 1 K (Augstein et al. 1974; Sarachik 1974). Because of this mixing, dry static energy is uniform beneath z_B, so that the first term on the left-hand side of (A3) and (A4), which represents subsidence warming of the layer, is set equal to zero.

Between the top of this layer at z_B and the tropopause at z_T, warming associated with adiabatic descent balances cooling by radiation, reevaporation of hydrometeors, and (within the nonconvecting region) export of heat to midlatitudes by atmospheric eddies ($F_{m,s}$ in watts per meter squared), so that the budgets of dry static energy are

$$a_wM_w(s_{B,w} - s_T) = a_w[R_w(z_T) - R_w(z_B) - M_wLl_{T,w} - L\mathcal{R}_w] \tag{A5}$$

$$a_cM_c(s_{B,c} - s_T) = a_c[R_c(z_T) - R_c(z_B) + F_{m,s} - M_cLl_{T,c} - L\mathcal{R}_c]. \tag{A6}$$

Cooling by the reevaporation of hydrometeors that descend from the detrainment level is given by $a_wM_wLl_{T,w} + a_wL\mathcal{R}_w$ and $a_cM_cLl_{T,c} + a_cL\mathcal{R}_c$. As described below with regard to the moisture budget, reevaporating hydrometeors are divided into two categories: those small enough to be carried by the large-scale circulation, whose flux is denoted by $a_wM_wl_{T,w}$ and $a_cM_cl_{T,c}$; and those larger hydrometeors that fall at a much faster speed and whose flux is denoted by $a_wL\mathcal{R}_w$ and $a_cL\mathcal{R}_c$. Because of dynamical effects, dry static energy is assumed to be horizontally uniform at the detrainment level.

b. Moisture budget

For the moisture budget, the lower layer is defined to extend from the surface to the top of the trade inversion at $z_{\rm TI}$. Recall that for the budgets of dry static energy the lower layer over the convecting and nonconvecting regions extends only to the lifting condensation level z_B. The use of different layer thicknesses for the dry static energy and moisture budgets is an accounting shortcut and does not represent any approximation. (We could have defined the top of the lower layer as z_B for budgets of both moisture and dry static energy. If we then constructed the moisture budget for the layer extending from z_B to the trade inversion and combined this with the lowest-layer moisture budget, we would have arrived at the same equations described below.)

The moisture budgets for the lower layer are

$$a_wM_w(q_{B,w} - q_{\rm TI,w}) + a_cM_c(q_{B,w} - q_{B,c}) = a_wE_w \tag{A7}$$

$$a_cM_c(q_{B,c} - q_{\rm TI,c}) = a_cE_c + a_cF_{m,q}, \tag{A8}$$

where the subscript ''TI'' refers to the value of specific humidity at the trade inversion. The evaporation rate E and the divergence of the eddy moisture flux $F_{m,q}$ are evaluated per unit area. Eddy divergence of moisture is assumed to occur entirely within the nonconvecting region, as before, and is neglected above the trade inversion.

We do not attempt to compute in detail the distribution of moisture above the trade inversion. Instead, we assume that relative humidity above the trade inversion decreases linearly with pressure, following Manabe and Weatherald (1967). Within the convecting region, relative humidity above the trade inversion decreases with respect to the surface value. Within the nonconvecting region, however, relative humidity decreases with respect to a value of the specific humidity that is specified

above the boundary layer as an external parameter of the model. As a consequence, upper-tropospheric moisture within the convecting region is coupled to thermodynamic conditions at the surface, while upper-tropospheric moisture within the nonconvecting region is held fixed.

While the vertical distribution of moisture above the boundary layer is given by the relative humidity profile assumed above, we can construct illustrative budgets of specific humidity q and liquid water l above the trade inversion. We assume that air subsiding from the tropopause is moistened by reevaporating hydrometeors (Sun and Lindzen 1993), although moistening by lateral advection (Salathe and Hartmann 1997; Yang and Pierrehumbert 1994; Pierrehumbert 1998) could be modeled using the same formalism. We distinguish between hydrometeors that are small enough to be carried along with the large-scale flow, and larger particles whose fall speeds are much higher. The latter are assumed to fall out of the flow at the tropopause at a rate denoted by $-a_w\mathcal{R}_w$ and $-a_c\mathcal{R}_c$, and reappear as water vapor at lower levels through evaporation. Thus, the budgets of specific humidity and liquid water at the tropopause are

$$a_w M_w l_{T,w} - a_c M_c l_{T,w} - a_u M_u l_{T,u} = -a_w \mathcal{R}_w \quad \text{(A9)}$$

$$a_u M_u (q_{T,w} - q_{T,u}) = 0, \quad \text{(A10)}$$

$$a_c M_c (l_{T,c} - l_{T,w}) = -a_c \mathcal{R}_c \quad \text{(A11)}$$

$$a_c M_c (q_{T,c} - q_{T,w}) = 0. \quad \text{(A12)}$$

Because the temperature of the tropopause is assumed to be horizontally uniform, water vapor does not condense while detraining laterally, so that $q_{T,c}$, $q_{T,w}$, and $q_{T,u}$ are equal.

All hydrometeors are assumed to evaporate completely before they reach the trade inversion. Thus, between the tropopause and trade inversion, the budgets of water vapor are

$$a_w M_w (q_{\mathrm{TI},w} - q_{T,w}) = a_w (\mathcal{R}_w + M_w l_{T,w}) \quad \text{(A13)}$$

$$a_c M_c (q_{\mathrm{TI},c} - q_{T,c}) = a_c (\mathcal{R}_c + M_c l_{T,c}). \quad \text{(A14)}$$

Given $q_{\mathrm{TI},w}$ and $q_{\mathrm{TI},c}$ (through specification of the convecting region relative humidity profile, and as an external variable, respectively), we can solve for the reevaporation rates that are needed for the free troposphere dry static energy budget.

Finally, the total precipitation $a_u P$ within the convecting region can be derived diagnostically, using the moisture budget for the updraft in the limit of vanishing a_u:

$$a_u M_u (q_{T,w} + l_{T,u} - q_{B,w}) = -a_u P. \quad \text{(A15)}$$

Using (A9)–(A14), we can relate the total water detrained at the top of the updraft to the water vapor subsiding through the trade inversion:

$$a_u M_u (q_{T,u} + l_{T,u}) = a_w M_w q_{\mathrm{TI},w} + a_c M_c q_{\mathrm{TI},c}. \quad \text{(A16)}$$

Thus, by prescribing the trade inversion moisture (either through the relative humidity profile in the convecting region or as an external variable in the nonconvecting region), we are equivalently prescribing the precipitation efficiency.

c. Surface energy balance and energy integrals

We add a surface energy budget,

$$R_w(0) - LE_w - S_w + F_{o,w} = 0 \quad \text{(A17)}$$

$$R_c(0) - LE_c - S_c + F_{o,c} = 0, \quad \text{(A18)}$$

where $F_{o,w}$ and $F_{o,c}$ represent the import of energy per unit area by the ocean circulation within the convecting and nonconvecting regions, respectively. Then it can be shown by summing over the vertical layers of the convecting and nonconvecting regions that

$$a_w R_w(z_T) + a_w F_{o,w} = a_c M_c (h_T - h_{B,c}) \quad \text{(A19)}$$

$$a_c R_c(z_T) + a_c F_{o,c} + a_c F_{m,h} = -a_c M_c (h_T - h_{B,c}), \quad (3)$$

where $F_{m,h}$ equals $F_{m,s} + LF_{m,q}$, the export of moist static energy to midlatitudes by atmospheric eddies. The quantity $h_T - h_{B,c}$ is identical to the gross moist stability derived by Neelin and Held (1987), who noted that in order for a direct circulation to export energy from an atmospheric column, the moist static energy must be larger in the outflow branch of the circulation.

d. External parameters

The budgets that are used to solve for temperature and moisture throughout the model domain depend upon various physical constants, along with the ocean and atmospheric eddy transports to midlatitudes, cloud radiative forcing, and the areal extent of the various regions, all of which are externally prescribed. Here we specify these quantities for two cases: an oceanic and a continental direct circulation. For the oceanic case, we compute the response to annually averaged radiative and eddy forcing, whereas NH summer solstice forcing is used for the continental case. For both cases, radiative fluxes are computed assuming the convecting region is centered at 4°N latitude, with the nonconvecting region centered at 20°N. The location of each region is held fixed in the model, although in reality these can change in response to dust radiative forcing at TOA. A change in location will alter the meridional circulation (Lindzen and Hou 1988), which may affect the surface temperature perturbation, although calculation of this sensitivity is beyond our model.

The use of ocean and land as a lower boundary results in contrasting choices of surface albedo; evaporation efficiency β; and ω_0, the coefficient of proportionality in the surface flux parameterization [cf. (1)]. Over ocean, the surface albedo depends upon the solar incidence angle but is typically less than 10%. The ocean albedo is computed automatically by the radiation model

TABLE A1. Summary of external parameters.

Prescribed variables	Symbol	Ocean case	Continental case
Fractional area			
Convecting region	a_w	0.4	0.4
Nonconvecting region	a_c	0.6	0.6
Surface albedo			
Convecting region	A_w	computed	0.15
Nonconvecting region	A_c	computed	0.35
Potential evaporation			
Convecting region	β_w	1.0	0.5
Nonconvecting region	β_c	1.0	0.15−0.01
Surface flux coefficient			
Convecting region	$\omega_{0,w}$	10^{-3} mb s^{-1}	3×10^{-3} mb s^{-1}
Nonconvecting region	$\omega_{0,c}$	10^{-3} mb s^{-1}	3×10^{-3} mb s^{-1}
Divergence by ocean heat transport			
Convecting region	$F_{o,w}$	−23.6 W m^{-2}	—
Nonconvecting region	$F_{o,c}$	−23.6 W m^{-2}	—
Divergence of atmospheric eddy			
Dry static energy transport			
Convecting region	—	—	—
Nonconvecting region	$F_{m,s}$	$(-8.6/a_c)$ W m^{-2}	$(-4.3/a_c)$ W m^{-2}
Divergence of atmospheric eddy			
Latent heat transport			
Convecting region	—	—	—
Nonconvecting region	$LF_{m,q}$	$(-10.2/a_c)$ W m^{-2}	$(-3.4/a_c)$ W m^{-2}
Trade inversion height			
Convecting region	$z_{\mathrm{TI},w}$	2.0 km	2.0 km
Nonconvecting region	$z_{\mathrm{TI},c}$	1.5 km	computed

and need not be specified. Over land, we chose for the convecting region, which is intended to resemble the Guinea coast of Africa, a value of 15%, while for the nonconvecting region, which is intended to resemble the desert region to the north, we set the albedo equal to 35% (e.g., Ramanathan et al. 1989). The evaporation efficiency β is unity over the ocean, but AGCM estimates suggest that 0.5 is a typical value along the lush Guinea coastal region. For the nonconvecting region, we allow β to vary between 0.15 and 0.01. The coefficient of proportionality ω_0 in the surface flux formulas [(1)] depends upon the drag coefficient, which is typically higher over land as a result of its dependence upon surface roughness, although this is somewhat offset by the larger surface wind speed over ocean regions. Following Betts and Ridgway (1989), we set the oceanic value of ω_0 equal to 0.001 mb s^{-1} and estimate from AGCM experiments that the appropriate land value is three times larger. For simplicity, we have set ω_0 equal to a constant value, independent of the strength of the circulation, thus excluding the ventilation feedback described by Hartmann and Michelsen (1993).

Atmospheric eddy transports are assumed to remove heat and moisture from the nonconvecting region. Eddy heat transport is observed to occur throughout the entire depth of the troposphere, but because the lower layer used to define the dry static energy budget is comparatively thin, we assume for simplicity that the transport occurs entirely between z_B and the tropopause. In contrast, eddy moisture transport is idealized to occur beneath the trade inversion. Heat is also exported from both the convective and nonconvecting regions by ocean transports. When the ocean is used as a lower boundary, the observed annually averaged ocean and atmospheric eddy transports are prescribed based upon Peixoto and Oort (1992). For the continental case, the ocean export is set to zero and the atmospheric eddy values are given NH summer averages appropriate for the Sahara–Arabian Desert region (Peixoto and Oort 1992). Precise values of these transports are listed in Table A1.

Cloud radiative forcing is held fixed in this model. The ISCCP climatology (Rossow and Schiffer 1991) suggests that cloud forcing in the nonconvecting region can be attributed to low clouds, whereas clouds associated with convective clusters dominate the radiative forcing within the convecting region. In addition, convective clouds are assumed to increase the radiative heating of the atmosphere, by reducing the net flux at the surface while leaving the net flux at the top of the atmosphere nearly unperturbed (e.g., Kiehl 1994). The precise values of cloud forcing used in the model are given in Miller (1997). The one exception is low cloud forcing in the nonconvecting branch for the continental case, which is reduced by a third from the oceanic value,

based upon ISCCP estimates over the Sahara–Arabian Desert region during NH summer. While cloud forcing is held fixed in this model for simplicity, we speculate about the semi-indirect feedback between aerosol amount and cloud cover that has been noted by Hansen et al. (1997).

The fractional area of the convecting region, a_w, is given the value of 0.4. As noted by Miller (1997), based upon ISCCP estimates of deep convective cloud cover, the boundary between the convecting and nonconvecting regions in the Tropics is fairly distinct, and while the location of convection changes from one season to the next, the fractional area undergoing deep convection is fairly constant.

The externally prescribed constants and boundary fluxes are summarized in Table A1.

e. Algorithm

To find solutions to the model, we begin by guessing for each region the temperature of the surface air and ocean (or ground), along with surface specific humidity. Using $T_{s,w}$ and $q_{B,w}$, we construct the moist adiabat linking the convecting region mixed layer and the tropopause. The height of the tropopause, z_T, is given by the level where the moist-adiabatic temperature equals the prescribed stratospheric temperature (set equal to 195 K). We also solve for $q_{T,u}$, assuming that air is saturated at the cloud top. Given our assumption of horizontally uniform temperature, the adiabat gives temperature everywhere above the trade inversion. Using the mixing line model, we can compute the temperature and moisture profiles between z_B, the top of the mixed layer (computed as the lifting condensation level), and the prescribed trade inversion height z_{TI}. The assumption that relative humidity decreases linearly with pressure above the boundary layer gives the remaining information needed to calculate the clear-sky radiative fluxes, which are augmented by the prescribed cloud forcing.

Using (A5), (A10), and (A13) along with (A6), (A12), and (A14), we can solve for the subsidence rates, M_w and M_c. Next we solve for the surface sensible heat fluxes, S_w and S_c, using the lower-layer dry static energy balances, (A3) and (A4). Similarly, we solve for the surface evaporation, E_w and E_c, using the lower-layer moisture balances, (A7) and (A8). Finally, we check whether the derived surface latent and sensible heat fluxes, along with the surface radiative fluxes and the prescribed ocean heat transports, satisfy the surface energy budgets, (A17) and (A18). We also check whether the derived surface latent and sensible heat fluxes are consistent with the values derived from the bulk parameterizations [(1)]. If not, our initial guesses for surface air and ground temperature, along with surface specific humidity, were incorrect and we have to choose new values and iterate until these constraints are satisfied. In summary, solving our simple tropical model is a root-finding problem consisting of six transcendental equations, with six unknowns: $T_{s,w}$, $T_{s,c}$, SST_w, SST_c, $q_{B,w}$, and $q_{B,c}$.

The independent variables of our model are the specific humidity at some level above the boundary layer of the nonconvecting region (at 5 km to be precise), along with β_c, the evaporation efficiency of this region for the continental case.

REFERENCES

Augstein, E., H. Schmidt, and F. Ostapoff, 1974: The vertical structure of the atmospheric planetary boundary layer in undisturbed trade winds over the Atlantic Ocean. *Bound.-Layer Meteor.,* **6,** 129–150.

Betts, A. K., 1982: Saturation point analysis of moist convective overturning. *J. Atmos. Sci.*, **39,** 1484–1505.

——, and W. Ridgway, 1989: Climatic equilibrium of the atmospheric convective boundary layer over a tropical ocean. *J. Atmos. Sci.*, **46,** 2621–2641.

Browning, K. A., and Coauthors, 1991: Environmental effects from burning oil wells in Kuwait. *Nature,* **351,** 363–367.

Carlson, T. N., and J. M. Prospero, 1972: The large-scale movement of Saharan air outbreaks over the northern equatorial Atlantic. *J. Appl. Meteor.*, **11,** 283–297.

Cess, R. D., G. L. Potter, S. J. Ghan, and W. L. Gates, 1985: The climatic effects of large injections of atmospheric smoke and dust: A study of climate feedback mechanisms with one- and three-dimensional climate models. *J. Geophys. Res.*, **90,** 12 937–12 950.

——, and Coauthors, 1995: Absorption of solar radiation by clouds: Observations versus models. *Science,* **267,** 496–499.

Charney, J. G., 1975: Dynamics of deserts and drought in the Sahel. *Quart. J. Roy. Meteor. Soc.,* **101,** 193–202.

Chou, M.-D., 1994: Radiation budgets in the western tropical Pacific. *J. Climate,* **7,** 1958–1971.

Coakley, J. A., and R. D. Cess, 1985: Response of the NCAR Community Climate Model to the radiative forcing by the naturally occuring tropospheric aerosol. *J. Atmos. Sci.,* **42,** 1677–1692.

Eliassen, A., 1951: Slow thermally or frictionally controlled meridional circulation in a circular vortex. *Astrophys. Norv.,* **5,** 19–60.

Emanuel, K. E., 1986: An air–sea interaction theory for tropical cyclones. Part I: Steady-state maintenance. *J. Atmos. Sci.,* **43,** 585–604.

Fang, M., and K. K. Tung, 1996: A simple model of nonlinear Hadley circulation with an ITCZ: Analytic and numerical solutions. *J. Atmos. Sci.,* **53,** 1241–1261.

Ghan, S. J., M. C. MacCracken, and J. J. Walton, 1988: Climatic response to large atmospheric smoke injections: Sensitivity studies with a tropospheric general circulation model. *J. Geophys. Res.,* **93,** 8315–8337.

Hansen, J., G. Russell, D. Rind, P. Stone, A. Lacis, S. Lebedeff, R. Ruedy, and L. Travis, 1983: Efficient three-dimensional global models for climate studies: Models I and II. *Mon. Wea. Rev.,* **111,** 609–662.

——, M. Sato, A. Lacis, and R. Ruedy, 1997: The missing climate forcing. *Philos. Trans. Roy. Soc. London,* **352B,** 231–240.

Hartmann, D. L., and M. L. Michelsen, 1993: Large-scale effects on the regulation of tropical sea surface temperature. *J. Climate,* **6,** 2049–2062.

Held, I. M., and A. Y. Hou, 1980: Nonlinearly axially symmetric circulations in a nearly inviscid atmosphere. *J. Atmos. Sci.,* **37,** 515–533.

Herman, J. R., P. K. Bhartia, O. Torres, C. Hsu, C. Seftor, and E. Celarier, 1997: Global distribution of UV-absorbing aerosols from Nimbus-7/TOMS data. *J. Geophys. Res.,* **102,** 16 911–16 922.

Houze, R. A., and A. K. Betts, 1981: Convection in GATE. *Rev. Geophys. Space Phys.,* **19,** 541–576.

Husar, R. B., J. M. Prospero, and L. L. Stowe, 1997: Characterization of tropospheric aerosols over the oceans with the NOAA Advanced Very High Resolution Radiometer optical thickness operational product. *J. Geophys. Res.,* **102,** 16 889–16 909.

Kalnay, E., and Coauthors, 1996: The NCEP/NCAR 40-Year Reanalysis Project. *Bull. Amer. Meteor. Soc.,* **77,** 437–471.

Kiehl, J. T., 1994: On the observed near cancellation between longwave and shortwave cloud forcing in tropical regions. *J. Climate,* **7,** 559–565.

Klein, S. A., and D. L. Hartmann, 1993: The seasonal cycle of low stratiform clouds. *J. Climate,* **6,** 1587–1606.

Lacis, A. A., and M. I. Mishchenko, 1995: Climate forcing, climate sensitivity, and climate response: A radiative modeling perspective on atmospheric aerosols. *Aerosol Forcing of Climate,* R. J. Charlson and J. Heintzenberg, Eds., John Wiley and Sons, 11–42.

Larson, K., D. L. Hartmann, and S. A. Klein, 1999: The role of clouds, water vapor, circulation, and boundary layer structure in the sensitivity of the tropical climate. *J. Climate,* in press.

Li, X., H. Maring, D. Savoie, K. Voss, and J. M. Prospero, 1996: Dominance of mineral dust in aerosol light-scattering in the North Atlantic trade winds. *Nature,* **380,** 416–419.

Lindzen, R. S., and A. Y. Hou, 1988: Hadley circulations for zonally averaged heating centered off the equator. *J. Atmos. Sci.,* **45,** 2416–2427.

——, A. Y. Hou, and B. F. Farrell, 1982: The role of convective model choice in calculating the climate impact of doubling CO_2. *J. Atmos. Sci.,* **39,** 1189–1205.

Manabe, S., and R. T. Weatherald, 1967: Thermal equilibrium of the atmosphere with convective adjustment. *J. Atmos. Sci.,* **24,** 241–259.

Miller, R. L., 1997: Tropical thermostats and low cloud cover. *J. Climate,* **10,** 409–440.

——, and I. Tegen, 1998: Climate response to soil dust aerosols. *J. Climate,* **11,** 3247–3267.

Mitchell, J. F. B., R. A. Davis, W. J. Ingram, and C. A. Senior, 1995: On surface temperature, greenhouse gases, and aerosols: Models and observations. *J. Climate,* **8,** 2364–2386.

Moulin, C., C. E. Lambert, F. Dulac, and U. Dayan, 1997: Control of atmospheric export of dust from North Africa by the North Atlantic Oscillation. *Nature,* **387,** 691–693.

Neelin, J. D., and I. M. Held, 1987: Modeling tropical convergence based on the moist static energy budget. *Mon. Wea. Rev.,* **115,** 3–12.

Peixoto, J. P., and A. H. Oort, 1992: *Physics of Climate.* American Institute of Physics, 520 pp.

Pierrehumbert, R. T., 1995: Thermostats, radiator fins, and the runaway greenhouse. *J. Atmos. Sci.,* **52,** 1784–1806.

——, 1998: Lateral mixing as a source of subtropical water vapor. *Geophys. Res. Lett.,* **25,** 151–154.

Prospero, J. M., and R. T. Nees, 1986: Impact of North African drought and El Niño on mineral dust in the Barbado trade winds. *Nature,* **320,** 735–738.

Ramanathan, V., and W. Collins, 1991: Thermodynamic regulation of ocean warming by cirrus clouds deduced from observations of the 1987 El Niño. *Nature,* **351,** 27–132.

——, R. D. Cess, E. F. Harrison, P. Minnis, B. R. Barkstrom, E. Ahmad, and D. L. Hartmann, 1989: Cloud-radiative forcing and climate: Results from the Earth Radiation Budget Experiment. *Science,* **243,** 57–63.

——, B. Subasilar, G. J. Zhang, W. Conant, R. D. Cess, J. T. Kiehl, H. Grassl, and L. Shi, 1995: Warm pool heat budget and shortwave cloud forcing: A missing physics? *Science,* **267,** 499–503.

Riehl, H., and J. S. Malkus, 1958: On the heat balance of the equatorial trough zone. *Contrib. Atmos. Phys.,* **52,** 503–538.

Rosenzweig, C., and F. Abramopoulos, 1997: Land-surface model development for the GISS GCM. *J. Climate,* **10,** 2040–2054.

Rossow, W. B., and R. A. Schiffer, 1991: ISCCP cloud data products. *Bull. Amer. Meteor. Soc.,* **72,** 2–20.

Salathe, E. P., and D. L. Hartmann, 1997: A trajectory analysis of tropical upper-tropospheric moisture and convection. *J. Climate,* **10,** 2533–2547.

Sarachik, E. S., 1974: The tropical mixed layer and cumulus parameterization. *J. Atmos. Sci.,* **31,** 2225–2230.

——, 1978: Tropical sea surface temperature: An interactive one-dimensional atmosphere–ocean model. *Dyn. Atmos. Oceans,* **2,** 455–469.

Schneider, E. K., 1977: Axially symmetric steady-state models of the basic state for instability and climate studies. Part II: Nonlinear calculations. *J. Atmos. Sci.,* **34,** 280–296.

——, 1983: Martian dust storms: Interpretive axially symmetric models. *Icarus,* **55,** 302–331.

Schubert, W. H., P. E. Ciesielski, C. Lu, and R. H. Johnson, 1995: Dynamical adjustment of the trade wind inversion layer. *J. Atmos. Sci.,* **52,** 2941–2952.

Slingo, J. M., 1980: A cloud parameterization scheme derived from GATE data for use with a numerical model. *Quart. J. Roy. Meteor. Soc.,* **106,** 747–770.

Sokolik, I. N., and O. Toon, 1996: Direct radiative forcing by anthropogenic airborne mineral aerosols. *Nature,* **381,** 681–683.

Sun, D.-Z., and R. S. Lindzen, 1993: Water vapor feedback and the ice age snowline record. *Ann. Geophys.,* **11,** 204–215.

——, and A. H. Oort, 1995: Humidity–temperature relationships in the tropical troposphere. *J. Climate,* **8,** 1974–1987.

Tegen, I., and I. Fung, 1994: Modeling of mineral dust in the atmosphere: Sources, transport, and optical thickness. *J. Geophys. Res.,* **99,** 22 897–22 914.

——, and ——, 1995: Contribution to the atmospheric mineral aerosol load from land surface modification. *J. Geophys. Res.,* **100,** 18 707–18 726.

——, and A. A. Lacis, 1996: Modeling of particle influence on the radiative properties of mineral dust aerosol. *J. Geophys. Res.,* **101,** 19 237–19 244.

——, and R. Miller, 1998: Mineral dust aerosols as an interactive tracer in an AGCM. *J. Geophys. Res.,* **103,** 25 975–25 995.

——, A. A. Lacis, and I. Fung, 1996: The influence on climate forcing of mineral aerosols from disturbed soils. *Nature,* **380,** 419–422.

——, P. Hollrig, M. Chin, I. Fung, D. Jacob, and J. Penner, 1997: Contribution of different aerosol species to the global aerosol extinction optical thickness: Estimates from model results. *J. Geophys. Res.,* **102,** 23 895–23 915.

Walker, J., and P. R. Rowntree, 1977: The effect of soil moisture on circulation and rainfall in a tropical models. *Quart. J. Roy. Meteor. Soc.,* **103,** 29–46.

Xu, K.-M., and K. A. Emanuel, 1989: Is the tropical atmosphere conditionally unstable? *Mon. Wea. Rev.,* **117,** 1471–1479.

Yang, H., and R. T. Pierrehumbert, 1994: Production of dry air by isentropic mixing. *J. Atmos. Sci.,* **51,** 3437–3454.